VILNIUS UNIVERSITY
CENTER FOR PHYSICAL SCIENCE AND TECHNOLOGY

Ignas Reklaitis

Advanced III-nitride-based optoelectronic devices: fabrication and characterization

Doctoral dissertation
Technological Science, Materials Engineering (08 T)

Vilnius 2016

Doctoral dissertation was prepared during the period of 2011-2015 years at Vilnius University Faculty of Physics and Institute of Applied Research.

Scientific supervisor – prof. dr. Roland Tomašiūnas (Vilnius University, Technological Science, Materials Engineering – 08 T).

VILNIAUS UNIVERSITETAS
FIZINIŲ IR TECHNOLOGIJOS MOKSLŲ CENTRAS

Ignas Reklaitis

Pažangių nitridinių optoelektronikos prietaisų kūrimas ir charakterizavimas

Daktaro disertacija
Technologijos mokslai, medžiagų inžinerija (08 T)

Vilnius 2016

Disertacija rengta 2011 – 2015 Vilniaus universiteto Taikomųjų mokslų institute bei Fizikos fakulteto Puslaidininkių fizikos katedroje.

Mokslinis vadovas – prof. dr. Roland Tomašiūnas (Vilniaus universitetas, technologijos mokslai, medžiagų inžinerija – 08 T).

Acknowledgements

First of all, I would like to thank my parents and brother for inspiration and support to start the doctoral studies. Then I would like to thank my undergrad and grad school supervisor prof. Artūras Žukauskas and advisor dr. Pranciškus Vitta. They've put a lot of effort to shape my experimental scientific skills. I'm very grateful to head of Semiconductor Physics Department prof. Gintautas Tamulaitis for encouragement during my study years. Finally, I would like to show my gratitude to my scientific supervisor of PhD studies, dr. Roland Tomašiūnas for accepting me as a PhD student, trust and support through out the studies.

I would like to thank most kindly to elder colleagues dr. Tadas Malinauskas, dr. Arūnas Kadys, dr. Tomas Grinys, Regina Beresnienė, Justinas Baužys, Gražina Medeišienė for warm atmosphere in our laboratory and the surrounding area. I acknowledge my younger colleagues Rolandas Kudžma, Aurina Arnatkevičiūtė, Mantas Dmukauskas, Morta Marcinkutė, Eglė Bašinskaitė and Bronislovas Razgus for contributing in my research as a part of their scientific research practice.

I acknowledge Lithuanian Research Council and Physics Faculty of Vilnius University for financially supporting the possibility to visit a number of the international scientific conferences and to participate in several internships. Moreover, I would like to thank prof. Evgenii Victorovich Lutsenko, prof. Michał Leszczynski, prof. Chih-Chung Yang and prof. Saulius Juodkazis, for accepting me in their research labs during my internships.

I would like to thank my buddy Andrius Janionis for language improvements.

Finally, I'm most grateful for my loving wife Monika Reklaitė for her endless support in the final and yet the most difficult part of my PhD studies - writing the dissertation.

Contents

Acknowledgements **v**

List of Abbreviations **viii**

Introduction **1**

1 Samples used in the study **12**

2 Frequency domain lifetime measurement study of "blue" and "green" InGaN LED structures **17**

2.1 Introduction 17

2.2 Experimental setup 19

2.2.1 Data processing 21

2.3 Experimental results 26

2.3.1 Temperature dependency 26

2.3.2 Photo-excitation power density dependency 32

2.4 Conclusions 35

3 Semi-planar III-nitride LED fabrication method by femtosecond ablation **36**

3.1 Introduction 36

3.2 Experimental setup 38

3.2.1 Masks fabrication 39

3.2.2 Devices processing 41

3.3 Experimental results 45

3.4 Conclusions 48

4 InGaN quantum well LED's ABC recombination coefficients revealed by the small signal frequency domain lifetime measurements **49**

4.1 Introduction 49

4.1.1 Theoretical background 51

4.2 Experimental setup 53

4.2.1 Electroluminescence measurements 53

4.2.2 Small-Signal Differential Carrier Lifetime measurements 53
4.3 Experimental results 55
4.4 Conclusions 60

5 Concluding summary 61

Bibliography 62

List of Abbreviations

AC	Alternating current
CW	Continuous wave
C*-*V	Capacitance-voltage characteristic
DC	Direct current
DLT	Differential carrier lifetime
EBE	Electron beam evaporator
EL	Electro luminescence
EQE	External quantum efficiency
FDLM	Frequency-domain lifetime measurement
FFT	Fast Fourier transform
fs	Femto second
IQE	Internal quantum efficiency
I*-*V	A current–voltage characteristic
LD	Laser diode
LED	Light emitting diode
LPF	Long pass filter
L*-*I	A light-current characteristic
MBE	Molecular beam epitaxy
MOCVD	Metalorganic chemical vapour deposition
MQW	Multiple quantum well
ns	Nano second
PL	Photo luminescence
PMT	Photo multiplier tube
ps	Pico second
QW	Quantum well
RIE	Reactive-ion etching
RTP	Rapid thermal processing
SEM	Scanning electron microscope
SPF	Short pass filter
SRH	Shockley–Read–Hall recombination
SSFDLM	Small-signal frequency-domain lifetime measurements
SSTRPL	Small-signal time-resolved photo luminescence

TRPL Time-resolved photo luminescence
XRD X-ray diffraction

Introduction

The world wide attention reached its peak to the III-group nitrides after an announcement of the Nobel Prize laureates in Physics of the year 2014 [1], which happened only 8 years after recognition of GaN technology by the Millennium Technology Prize in 2006. However it was long before that when attention to the topic began to grow. Since 1980's there were attempts to find a wide band gap semiconductors suitable for an optoelectronic or high power devices fabrication. GaN got the most attention, among other semiconductor materials such as silicon carbide, zinc oxide, zinc selenide and diamond, mainly because it is more stable compared to ZnO or ZnSe and it is easier to dope it compared to SiC or a diamond. Nevertheless, the technology of GaN devices, despite the fact of the Nobel price winning and commercial availability of GaN devices, is far from perfect.

One of the main difficulties in terms of GaN technology is a lack of native substrates for a homoepitaxial growth. It led to a heteroepitaxy of GaN, most commonly on a sapphire or less popular on a silicon carbide substrates. Both of them have pros and cons, the lattice constants and the thermal expansion coefficients of both differ significantly from the GaN, which result to an epitaxial layers with built-in tensions, high dislocation densities and even layer cracking. At the begging of the new millennium, the growth of GaN on silicon substrates was introduced and nowadays it becomes the dominant substrate used, despite a fact that it is even less suitable for GaN growth. The main advantages of this substrate are the low price, substrate compatibility with silicon integrated circuits or the possibility to remove substrate after epitaxial growth by cost effective selective wet chemical etching process.

The main GaN market, the production of InGaN/GaN MQW based LEDs for both niche and general lightning applications, is booming. The devices are based on an electroluminescence phenomena, first observed more than a 100 years ago by H. J. Round and he summarized the observation results in a paper published in 1907 [2]. The phenomena was then studied in more detail by O. V. Losev in 1928 [3]. Discovery of modern LED has been delayed for another 34 years until in 1962 several independent groups of scientist in the United States of America simultaneously reported about a

semiconductor laser pumped optically by a gallium arsenide LEDs.

Modern LEDs are about to celebrate their 55th anniversary, however the characterization techniques of bulk GaN wafers in order to judge their quality for a production line is still open for the debates. Most common wafer level characterization involves traditional structural (SEM, XRD etc), electrical (C-V profiling, Hall measurements) and optical (time integrated and time resolved PL) techniques. One of the easiest to interpret and perform are a PL measurements, which combined with the time-resolved capability is able to give good insight into the sample's properties. TRPL measurements are usually performed using a short pulses laser. However pulse fluence of lasers used to excite the sample creates non-equilibrium carriers concentration orders of magnitude higher than those achieved in working LED sample. Therefore, the characterization of a wafer structure, which will then be fabricated into an LED, is somewhat inaccurate. A good alternative to obtain the same experimental measure of sample properties is to perform frequency resolved PL measurements. Usually wide band gap LEDs are used as an excitation source for FDLM as they are cheap, stable and directly modulable light sources. One of the main advantages of FDLM is a *quasi*-CW excitation, which is more native to the device working situation, compared to the pulsed laser excitation. The only drawback of LEDs are their low output power, which, in this case, creates non-equilibrium carriers concentration orders of magnitude lower compared to those achieved in a typical high brightness LED working regime. The creation of measurement technique that is capable to fill-up the gap between two extreme cases, the LED for FDLM or the pulsed laser excitation for TRPL, making measurement excitation power density comparable to the actual LED working condition have a high impact on InGaN based LED structures wafer level characterization. Part of the research presented in this dissertation is dealing with this issue and results are compared to those obtained using widely established TRPL measurement method.

If the epi-wafer after characterization is approved for production line, the fabrication of devices takes place. Amano first attempts to make a GaN based diode had a geometry where ***p***-type contact is evaporated on the top surface, while ***n***-type contact is on the side wall of the epitaxial structure. Such an approach is a good alternative for a fast test of the devices, however is very inefficient in the case of a mass production. It hasn't been long after

a dry etching technique was introduced into a GaN LEDs fabrication process in order to attain planar fabrication geometry. Later, even more complex fabrication methods appeared as scientific attention increased. Vertical die geometry using SiC substrates to grow LEDs, sapphire substrate flip-chip, laser lift-off of sapphire substrate or selective wet chemical etching of silicon substrate enabled to develop thin film or even thin film flip chip diode die fabrication methods, however all of them have common multipliers - utilization of expensive and time consuming photo-lithography process. It pays off if a mass production takes place. However the photo-lithography masks costs treasure when a niche device must be fabricated, or better chip geometry should be developed, thus such approach becomes very impractical. R&D laboratories all over the world are searching for an inexpensive prototyping or a small batch fabrication methods, capable to produce custom die geometries fast and at a reduced price. The author of this dissertation was able to suggest his own fabrication process addressing this field and compared the performance of the fabricated device to the sample made using conventional fabrication method.

When it comes to the fabricated device characterisation, there is a variety of device performance evaluation tools. Most common of them are *I-V*, *L-I*, EQE, EL measurements. The main debate nowadays, in terms of the InGaN based LEDs performance, is the droop (the gradual decrease of efficiency of LED while increasing forward current) phenomena. It is widely believed that the origin of the droop is closely related to the Auger recombination. Thus, it would be attractive to consider an experimental technique enabling to optimize the Auger recombination coefficient, among Shockley-Read-Hall and bimolecular recombination coefficients, in order to evaluate device's performance. Such a tool already exists - the SSTRPL technique, which enables to evaluate the EQE and the ABC coefficients of the working LED sample without the need to perform measurements in absolute units, e.g. no need to use Ulbricht sphere and calibrated measurement tools. However the method is time consuming and needs an expensive excitation source and light detector. Further development of the technique in order to make it even more robust would be favourable in the GaN scientist community. For this purpose the Author adapted the FDLM setup to make it suitable for measuring the properties of working LED samples under small-signal regime.

Motivation

Goal of the work

The goal of this work is to develop improvements of existing fabrication and measurement methods in InGaN LED processing, including: novel wafer level characterization technique, improved LED fabrication process and evaluation of processed LED's performance.

Tasks of the dissertation

In order to fulfil the stated goal of this work the following tasks were set:

1. Development and implementation of novel frequency-resolved wafer level InGaN LED structure characterization technique. Established requirements for the technique - a resonant excitation of quantum wells, optical excitation power density must be comparable to the power densities achieved in a working LED and inexpensive implementation.

2. Reduction of an LED prototyping costs by adopting direct ultra-short pulse laser ablation instead of expensive and time consuming photolithography technique.

3. Establish an inexpensive and fast approach to evaluate the Shockley-Read-Hall, radiative and Auger recombination coefficients of a working LED device, in order to test its performance.

Novelty and importance of this work

In this work, two extreme cases of InGaN/GaN MQW samples, emitting in the green and blue spectral range, have been investigated using frequency domain lifetime measurement setup. It utilizes violet laser diode as a resonant excitation source, enables measuring sample properties within MQW region at the excitation power densities comparable to those obtained in working LED.

The use of a femtosecond laser and implementation of direct semi-planar LED ablation geometry enabled to fabricate working InGaN based LED

prototype with custom die geometry faster, while avoids manufacturing expensive photo-lithography masks.

Implementation of small signal frequency domain lifetime measurement setup enabled to measure differential carrier lifetimes of working LED both faster and in a wider forward current range than it is possible to achieve by the small signal time resolved photoluminescence method. The suggested SSFDLM setup is also less expensive compared to the SSTRPL.

Key statements for defence

1. The application of violet LD, instead of LED, in frequency domain lifetime measurement setup enables broadening excitation power density range up to 15 W/cm^2, making it more relevant for LED wafer characterization.

2. The use of fs laser ablation in a semi-planar geometry enables producing a working InGaN/GaN LED sample more robust and faster, by avoiding the use of expensive photolithography mask production and reducing the number of critical mask alignment and exposure production steps, as in the case of conventional LED processing.

3. The newly developed small signal frequency domain lifetime measurement technique reliably extracts recombination coefficients corresponding to the Shockley-Read-Hall, radiative and Auger recombination channels, of working LED sample while being both cheaper and more simple to operate than the common DLT measurement approaches.

Layout of the dissertation

A short introduction dealing with the goal and novelty of the work and author's contribution starts the dissertation, followed by a chapter about the samples used for the investigation. Three following chapters dedicated to discuss the main results achieved during a PhD studies and each are divided into smaller subsections. Each of the chapters consists of a short introduction, presentation of the experimental technique used, obtained experimental results and relevant conclusions at the end of the chapter.

The first chapter discusses wafer level characterization technique of an InGaN LED structure.

The second chapter is devoted to the LED prototyping approach using femtosecond laser ablation and semi-planar geometry.

The third chapter is dealing with the LED device characterization using small signal frequency domain approach.

Conclusions of all three individual chapters are then summarized. All the references that are quoted in the text are at the end of the dissertation.

Contribution of the author

The author's main contribution to this work is the creation, implementation and application of:

1. A characterization method, for a InGaN/GaN wafer characterization with a quantum well structures, using the frequency domain technique with a resonant violet laser diode excitation;

2. Novel GaN light emitting diode prototyping method using an ultra-short laser pulses and a semi-planar mesa ablation geometry;

3. An InGaN/GaN LED recombination coefficient evaluation method based on measuring the differential carrier lifetime of working InGaN/GaN LED sample while exciting it resonantly with a violet laser diode.

The author performed majority of experiments presented in the dissertation by him self or with a help of a junior colleague Rolandas Kudžma, the author also executed experimental data analysis and made following interpretations. The conclusions of the dissertation were achieved by the author's discussion with his senior colleagues, mainly with the supervisor of the doctoral studies dr. Roland Tomašiūnas and senior colleague dr. Tadas Malinauskas. The author extensively used the frequency domain measurement set-up which was already developed at the Insitute of Applied research by dr. P. Vitta, however adopted it in order to fulfil the goals of this work.

The author's carried out research allowed to summarize his results in four scientific publications related to the dissertation, three of them are already published. The author has also contributed to the preparation of a number

of scientific posters presented at the national and international scientific conferences, some of which he has presented by himself. The author is grateful to all co-authors who helped to perform scientific experiments and improve quality of both, scientific publications and conference posters.

Namely for dr. I. Pietzonka and dr. M. Strassburg (OSRAM Opto-semicondutors GmbH) for providing the sample used for the experiments represented in chapter 2, also for dr. S. Miasojedovas for helping to measure TRPL kinetics, to dr. P. Vitta and prof. A. Žukauskas for valuable comments and suggestions on the experimental results. In the case of LED fabrication (chapter 3), the sample wafer was commercially grown by Nitride Semiconductors Co. Ltd. The author is thankful to T. Puodžiūnas, L. Mažulė for making molybdenum masks in the lab of prof. V. Sirutkaitis (Laser Research Center, Vilnius University) which were used for contacts deposition, also to C.H. Lin who helped the author to make a conventional LED sample in the lab of prof. C.C. Yang (Taiwan at Institute of Photonics and Optoelectronics of National Taiwan University), to dr. A. Bičiūnas working in prof. A. Krotkus lab (Center for Physical Sciences and Technology), for several LED metallization experiments, finally to dr. T. Grinys who gave valuable suggestions on sample characterization. Chapter 4 which is dedicated to the study on ABC coefficients would have never been completed without the help of dr. H. Lugauer, dr. I. Pietzonka and dr. M. Strassburg (OSRAM Opto-semicondutors GmbH) who provided the examinated sample. SSTRPL measurements were performed by F. Nippert in the lab of prof. A. Hoffmann (Technische Universität Berlin). In collaboration with dr. S. Karpov the discussion of the results was improved remarkably.

The author acknowledges that this dissertation would have never been finished without contribution of his colleagues, listed as co-authors in the publications related to the dissertation.

Approbation of the research results

Essential part of the results presented in this work is published in the peer-reviewed scientific journals. Initial results of the ongoing research were presented in fifteen international and national conferences. The list of scientific papers and main conferences related to the dissertation is given below.

The list of 11 publications that were published during doctoral studies, but are not directly related by subject to the doctoral thesis, are also presented in a separate list.

List of publications related to the dissertation

[P1] A. Arnatkevičiūtė, **I. Reklaitis**, A. Kadys, T. Malinauskas, G. Juška, M.V. Rzheutski, and R. Tomašiūnas, Relationships between strain and recombination in intermediate growth stages of GaN, J. Electron. Mater. **43**(7), 2667 (2014).

[P2] **I. Reklaitis**, R. Kudžma, S. Miasojedovas, P. Vitta, A. Žukauskas, R. Tomašiūnas, I. Pietzonka, M. Strassburg „Photoluminescence decay dynamics in "blue" and "green" InGaN LED structures revealed by frequency domain technique", J. Electron. Mater. 45(7), 3290 (2016).

[P3] **I. Reklaitis**, T. Grinys, R. Tomašiūnas, T. Puodžiūnas, L. Mažulė, V. Sirutkaitis, C.H. Lin, C.C. Yang, A new geometrical approach for rapid LED processing by using femtosecond laser, Opt. Lasers Eng. **74**, 17 (2015).

[P4] **I. Reklaitis**, F. Nippert, R. Kudžma, T. Malinauskas, S. Karpov, I. Pietzonka, H.J. Lugauer, M. Strassburg, P. Vitta, R. Tomašiūnas, A. Hoffmann, Differential carrier lifetime in InGaN-based light-emitting diodes obtained by small-signal frequency-domain measurements: Advantages and limitations of the technique, submitted to the Meas. Sci. Technol.

List of conference contributions related to the dissertation

[C1] E.V. Lutsenko, M.V. Rzheutski, V.N. Pavlovskii, G.P. Yablonskii, **I. Reklaitis**, A. Kadys, T. Malinauskas, S. Nargelas, K. Jarašiūnas, and A. Žukauskas, "Peculiarities of photoluminescence efficiency dependence on excitation intensity in GaN/Al2O3 epilayers", *4th Int. Symp. on Growth of III-Nitrides* (St. Petersburg, July 16-19, 2012).

[C2] A. Kadys, T. Malinauskas, T. Grinys, **I. Reklaitis**, M. Dmukauskas, J. Mickevičius, J. Aleknavičius, D. Dobrovolskis G. Tamulaitis, and R. Tomašiūnas, "Growth of InN and InGaN thin films on GaN templates by pulsed MOCVD", *COST Spring training school „Epitaxy and structural analysis of III-V-N semiconductor nanostructures*", (Heraklion, April 29-May 2, 2012).

[C3] T. Grinys, A. Kadys, **I. Reklaitis**, M. Ščiuka, A. Melninkaitis, and R. Tomašiūnas, „Damage morphology stufy of GaN structures by electron beam induced current", *10th International Conference on Nitride Semiconductors* (Washington, August 25-30, 2013).

[C4] **I. Reklaitis**, R. Kudzma, R. Tomasiunas "Luminescence Decay Kinetics in InGaN Studied by Frequency Domain Measurements", *FP7 Spring training school* (Rome, april 7-11, 2014).

[C5] **I. Reklaitis**, T. Puodziunas, L. Mazule, T. Grinys, and R. Tomasiunas, "LED processing using fs lasermicrofabrication: playing with geometry" *5th Int. Symp. on Growth of III-Nitrides* (Atlanta, May 18-22, 2014).

[C6] **I. Reklaitis**, T. Puodziunas, L. Mazule, R. Tomasiunas, and V. Sirutkaitis, "Femtosecond Laser Processing of GaN Based LED Using 45 Degree Geometry" *International Workshop on Nitride Semiconductors 2014* (Wrocław , August 24-29).

[C7] J.Vaitkus, E.Gaubas, T.Ceponis, J.Pavlov, **I.Reklaitis**, "Transient signals of the capacitor and Schottky barrier type HVPE and MOCVD GaN sensors" *17th International Workshop on Radiation Imaging D* (Hamburg, 8 June-2 July 2015).

[C8] **I. Reklaitis**, R. Kudzma, R. Tomasiunas, I. Pietzonka, I. Titkov, E. Rafailov, "Blue and green LED structures investigated by photoluminescence frequency domain technique" *11th International Conference On Nitride Semiconductors* (Beijing, 30 August – 4 September 2015).

[C9] **I. Reklaitis**, R. Kudzma, R. Tomasiunas, I. Pietzonka, M. Strassburg. Photoluminescence frequency domain technique – a tool to investigate InGaN LED structures in a wide range of excitation and

time. *6th International Symposium on Growth of III-Nitrides (ISGN-6)* (Hamamatsu, November 8-13, 2015).

Publications not included in the dissertation

[N1] P. Vitta, R. Stanikūnas, A. Tuzikas, **I. Reklaitis**, A. Stonkus, A. Petrulis, H.P. Vaitkevičius, A. Žukauskas, Energy-saving approaches to solid state street lighting, Proc. SPIE **8123**, 81231H (2011).

[N2] P. Vitta, **I. Reklaitis**, A. Žukauskas, Frequency-domain fluorometry in the presence of high in-phase background, Meas. Sci. Tecnol. **23**, 035502 (2012).

[N3] E.V. Lutsenko, M.V. Rzeutski, V.Z. Zubialevich, V.N. Pavlovskii, G.P. Yablonskii, A.S. Shulenkov, **I. Reklaitis**, A. Kadys, T. Malinauskas, S. Nargelas, K. Jarašiūnas, A. Žukauskas, Peculiarities of photoluminescence efficiency dependence on excitation intensity in GaN/Al2O3 epilayers, Phys. Status Solidi C **10**, 511 (2013).

[N4] E.V. Lutsenko, M.V. Rzeutski, V.N. Pavlovskii, G.P. Yablonskii, **I. Reklaitis**, A. Kadys, A. Žukauskas, Relationship of quantum-well potential profile and luminescence of InGaN/GaN heterostructures, J. Appl. Spectrosc. **80**, 220 (2013).

[N5] T. Grinys, E. Jelmakas, **I. Reklaitis**, S. Lapinskas, A. Kadys, T. Malinauskas, C.C. Yang, R. Tomašiūnas, Defect study of GaN based LED structure by electron beam induced current, Phys. Status Solidi C **11**(3-4), 734 (2014).

[N6] K. Aponiene, E. Paskeviciute, **I. Reklaitis**, Z. Luksiene, Reduction of microbial contamination of fruits and vegetables by hypericin-based photosensitization: Comparison with other emerging antimicrobial treatments, J. Food Eng. **144**, 29 (2015).

[N7] A. Kadys, T. Malinauskas, M. Dmukauskas, **I. Reklaitis**, K. Nomeika, V. Gudelis, R. Aleksiejūnas, P. Ščajev, S. Nargelas, S. Miasojedovas, K. Jarašiūnas, Photoluminescence features and carrier dynamics in InGaN heterostructures with wide staircase interlayers and differently shaped quantum wells, Lith. J. Phys. **54**(3), 187 (2014).

[N8] T. Grinys, R. Dargis, A. Kalpakovaitė, A. Clark, F.E. Arkun, **I. Reklaitis**, R. Tomašiūnas, Study of GaN growth on Si with rare-earth oxide distributed Bragg reflector structures, J. Cryst. Growth **424**, 28 (2015).

[N9] I. Buchovec, V. Lukseviciute, A. Marsalka, **I. Reklaitis**, Z. Luksiene, Effective photosensitization-based inactivation of Gram (−) food pathogens and molds using the chlorophyllin–chitosan complex: towards photoactive edible coatings to preserve strawberries, Photochem. Photobiol. Sci. **15**, 506 (2016).

[N10] E. Gaubas, T. Ceponis, E. Kuokstis, D. Meskauskaite, J. Pavlov, **I. Reklaitis**, Study of Charge Carrier Transport in GaN Sensors, Mater. **9**, 293 (2016).

[N11] J. Pavlov, T. Čeponis, E. Gaubas, D. Meskauskaite, **I. Reklaitis**, J. Vaitkus, R. Grigonis, V. Sirutkaitis, Comparative study of deep levels in HVPE and MOCVD GaN by combining O-DLTS and pulsed photo-ionization spectroscopy, accepted by J. Instrum.

1. Samples used in the study

There were no state-of-the-art semiconductor growth tools in Lithuania until recently. However there are many scientific groups making their research on semiconductor characterization. It may seem odd that a lot of research is being done while there is no capabilities to make produce semiconductor samples in Lithuania. The simple explanation behind that is group leading professors' visits to international scientific conferences to make relationships with scientists from other regions and gain some samples for the investigation from them. Usually the samples are collected from different batches or their growing parameters are kept in secret, making it difficult to produce high impact publications. This led to a draft in Lithuania's scientific community to produce their very own semiconductor samples for the research. In 2009 compound semiconductor epitaxial growth machines started emerging one after another. In 2009 prof. Krotkus group have launched their second MBE reactor for GaAs growth, following year first GaN wafer was grown using MOCVD reactor in Vilnius University, at the begining of the year 2013 it was announced that first commercial AlGaAsSb wafer was grown in UAB Brolis Semiconductors using their MBE reactor, the launch of a new MBE tool of prof. Krotkus group is scheduled at the mid-2016. However there was little to no knowledge of semiconductor growth in Lithuania before 2009, especially in wide-band-gap semiconductor growth. It leads to a situation when all the knowledge, even most basic one, is usually gained via time and resources consuming trial and error method.

The initial guideline of this work, was to use the III-nitride based epitaxial layers grown using MOCVD reactor of Institute of Applied Research. However, despite the enormous efforts and sacrifices dr. A. Kadys and dr. T. Grinys have put into growing state-of-the-art structures, required samples haven't been grown. It resulted into the *status-quo* situation when competitive research can't be done as there were no structures to work on, while the days kept passing by and the end of PhD studies was approaching fast. This situation was overcome, by a decade old tradition of Lithuanian scientist community - the samples have been gathered elsewhere. Several samples arrived from fellow consortium OSRAM Opto Semicondutors, they have been used for wafer level and working LED characterization experi-

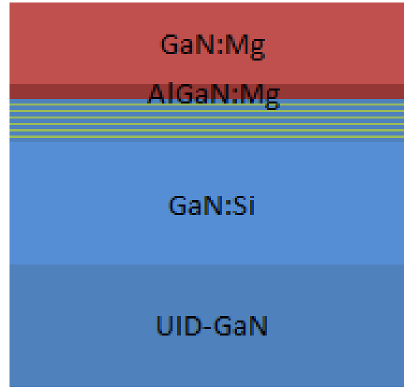

Figure 1.1 Indicative structure of samples used in the study. Top-to-bottom: *p*-type Mg doped GaN layer (100-150 nm thick), Mg doped electron blocking AlGaN layer (10-20 nm thick), x5 5 nm thick GaN barrier and 3 nm thick InGaN quantum well, *n*-type Si doped GaN (1000-1500 nm thick), unintentionally doped GaN buffer (1000-1500 nm thick) and c-plane (0001) sapphire substrate (not shown).

ments, while a single wafer was bought from company Nitride Semiconductors Co. Ltd for an LED fabrication. This, however, led to a situation where all samples used in the study, have two common multipliers:

1. all of the samples are III-nitride device structures or the LED device, MOCVD grown on a sapphire substrate;

2. all of them are commercial products, so little was revealed regarding their growing parameters.

Despite the fact that an exact structure of samples investigated was not provided, indicative structure is shown in figure 1.1, based on a knowledge of scientist from the Institute of Applied Research. Such a stalemate situation, then exact growth regime of epitaxial structures isn't known, made it difficult to talk about the physics behind the processes revealed by the research, however enabled to focus on the technological processes, instead. Creation and development of simple techniques capable to compare several samples and then judge which of them is better, or in the case of sample fabrication, focus on the processing itself rather than on the properties of the finished device.

Samples used for wafer level characterization

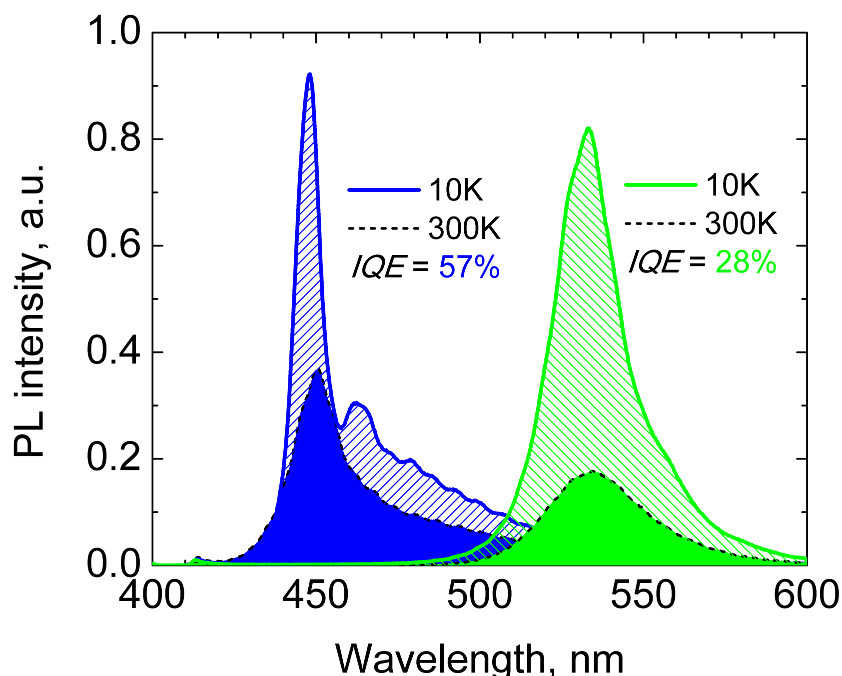

Figure 1.2 PL emission spectra of the investigated "blue" and "green" InGaN/GaN LED structures obtained using a violet LD as an excitation source (peak 405 nm) under the excitation power density of 50 mW/cm^2. Filled areas represent measurements performed at room temperature, while hatched areas represent measurements at 10 K temperature for both, "blue" and "green", samples [P2].

Two InGaN/GaN state-of-the-art LED test structures were provided from a partner of European Union FP7-ICT project No. FP7-318388 "NEWLED". Both of them have been MOCVD grown on a sapphire substrates in OSRAM Opto Semiconductors GmbH, Germany. The samples emitted light in the blue and green (further in the text samples are named as "blue" and "green" samples) spectral range with the characteristic peak wavelength of 450 nm and 530 nm, respectively. The samples consisted of a standard sequence of epi-layers for LED: buffer layer (unintentionally n-doped GaN), n-type GaN, active layer (stack of five MQWs with a typical 3 nm well width and indium content in it depending on the emission wavelength; >20 % for the 530 nm, wasn't specified in the case of the "blue" one), electron blocking layer and p-type GaN. The PL emission spectra of the samples are shown in figure 1.2. The evaluated internal quantum efficiency values are 57 % for

the “blue” one and 28 % for the “green” sample.

Structure used for the LED fabrication

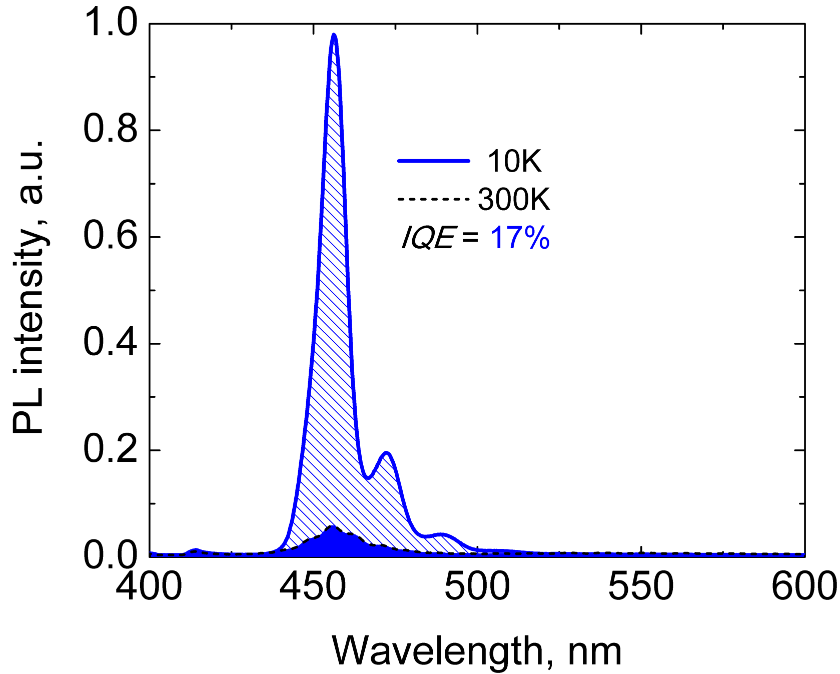

Figure 1.3 PL emission spectra of the LED structure used for LED fabrication. PL spectrum is obtained using a violet LD as an excitation source (peak 405 nm) under the excitation power density of 50 mW/cm^2. Blue color filled area represent measurement performed at room temperature, while hatched area represent measurement at 10 K temperature.

The wafer used for the LED fabrication experiments was bought from Nitride Semiconductors Co. Ltd., Japan. An active layer of the sample was based on five InGaN/GaN quantum wells, that were MOCVD grown on c-plane sapphire substrate. The reference LED sample was made by using conventional photolithography and dry etching process based on a Cl_2 and Ar plasma, discussed in more detail in subsection 3.2.2. An evaluated IQE of the sample was 17 % (see fig. 1.3).

Sample used for the working LED characterization experiments

Single state-of-the-art LED structure was grown by MOCVD epitaxy on a c-plane sapphire substrate, fabricated in to the LED and packaged by the OSRAM Opto Semiconductors GmbH. The sample was deliberately made so that measurement results obtained using SSFDLM and SSTRPL techniques could be compared. An active region of the structure consisted of five InGaN quantum wells (QWs) with a nominal thickness of 3 nm sandwiched between GaN barriers. The LED sample was mounted in the commercial Golden Dragon+ package, its emission peaked at 445 nm (see Fig. 1.4).

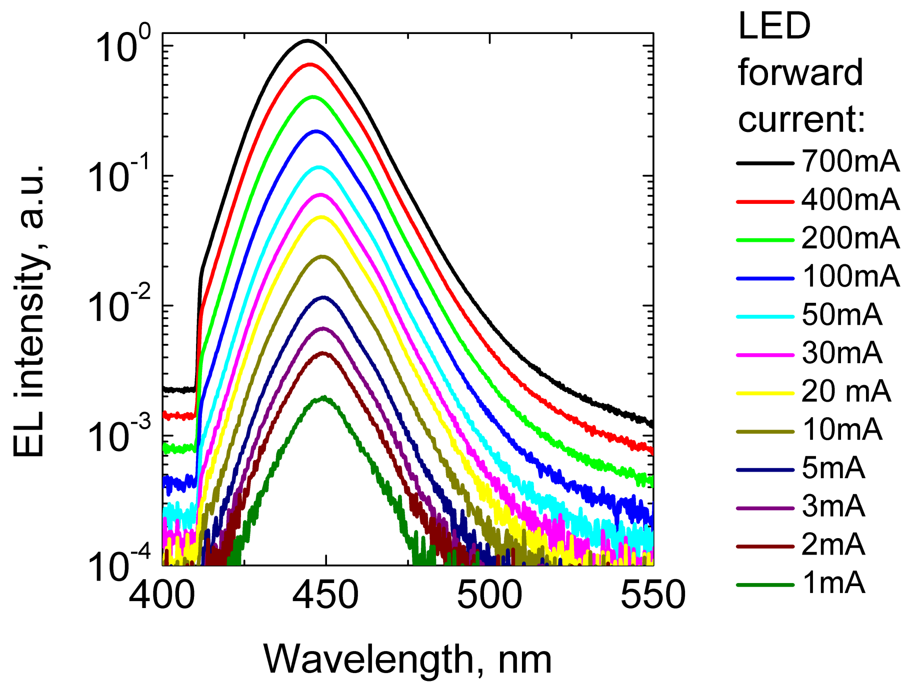

Figure 1.4 EL emission spectra of the LED sample investigated. An artefact observed in all spectrum bellow 410 nm is due to a LPF was used in the measurement setup.

2. Frequency domain lifetime measurement study of “blue” and “green” InGaN LED structures

2.1 Introduction

Measurements in the frequency domain has been the first technique for evaluating fluorescence lifetimes and was proposed by Gaviola in 1926 [4]. However, a lack of appropriate excitation sources with short emission wavelengths and difficulties to modulate them limited the use of this technique at that time. After the introduction of high-intensity flash lamps and short-pulse lasers, the time-resolved methods started dominating decay time measurements. There were few attempts to use CW lasers with external acousto-optic modulators emerged [5, 6, 7, 8] in the frequency-resolved fluorometry, however the external modulators have a drawback of narrow modulation frequency range and high cost. Only after the invention of wide-band-gap light-emitting diodes (LEDs), publications on lifetime measurements using frequency domain technique appeared again [9]. Moreover, frequency domain imaging based on a LED source has been developed [10]. The only isue with LED as an excitation source, despite its low noice and low cost, is the lack of output power. This drawback can be overcome by violet laser diode used in Blu-RayDisck ™technology – compact, stable, relatively high power and directly modulated excitation source. First attempts to use laser diodes in phase resolved fluorometry involved the investigation of Alq3 in chlorobenzene [11] and rhodamine 6G [12, 13], however it wasn’t ever applied for a wide-band-gap semiconductor characterization.

It is well known that frequency domain and time domain are related via Fourier transform [14] implying the fact that both techniques provides generally the same information. However, in the case of frequency domain lifetime measurement excitation source is working in *quasi*-CW regime, making

it easier to control and evaluate excitation power density within a sample. Frequency domain wasn't widely applied to a semiconductor investigations so far, mainly due to a lack of sufficiently powerful and cheap excitation source. Only a number of papers have been published on AlGaAs and InGaAsP heterostructures providing non-equilibrium carrier lifetimes in the microsecond and sub-microsecond range [15]. Few papers appeared on GaN related structures and devices [16], reporting that the technique allows performing measurements at extremely low excitation power densities (e.g., 0.5 mW/cm^2), and thus the study of competition between recombination mechanisms responsible for the yellow luminescence (YL) at charge carrier densities below saturation of recombination channels has become possible. However that is not even near the actual excitation power densities achieved in typical working LED, thus such experiments doesn't make desirable impact in InGaN/GaN LED wafer characterization.

Time domain measurements are more common among III-nitrides characterization [17, 18], however, usually high fluences are used for the excitation. Much higher than those obtained in working condition of the LED. Such over excitation might result in quenched parasitic recombination channels and thus some information about sample quality might be lost. Another draw back of the technique is pulsed excitation, which is not native to the typical LED application, e.g. general lighting.

As for Lithuania, there are several groups working on GaN. Prof. G. Tamulaitis is leading a group of scientist who specialise in characterization of GaN [19] InGaN [20] or even AlGaN [21] and BGaN [22] by using temperature dependent PL as their investigation tool. Prof. S. Juršėnas leads a group of researchers who uses time-resolved PL to investigate the GaN samples [23, 24]. Research on GaN in frequency-resolved PL for the time was one of the main topics of prof. A. Žukauskas and his team [25, 26]. There are even more exotic tools used in Lithuania. Prof. K. Jarašiūnas is leading a group who uses light induced transient grating method with even higher excitation than those typical for the TRPL to evaluate carrier lifetime and diffusion coefficient simultaneously by a single measurement [27, 28]. Prof. E. Gaubas team is analyzing defects in GaN epitaxial layers using microwaves [29, 30], while dr. A. Mekys uses Hall measurements for samples characterization [31].

It may seem that there is little to add to a number of methods described

above, however in terms of GaN structure characterization as an LED fabrication material, all of the methods described use excitation levels that are far from an actual working LED, thus making the characterization results somewhat irrelevant. The author of this disertation was able to adapt the FDLM setup previously used by dr. P. Vitta [32], while applying violet laser diode for resonant sample excitation. It enabled achieving a wide range of optically pumped carrier concentration, even up to those typical for working LEDs (15 W/cm^2).

2.2 Experimental setup

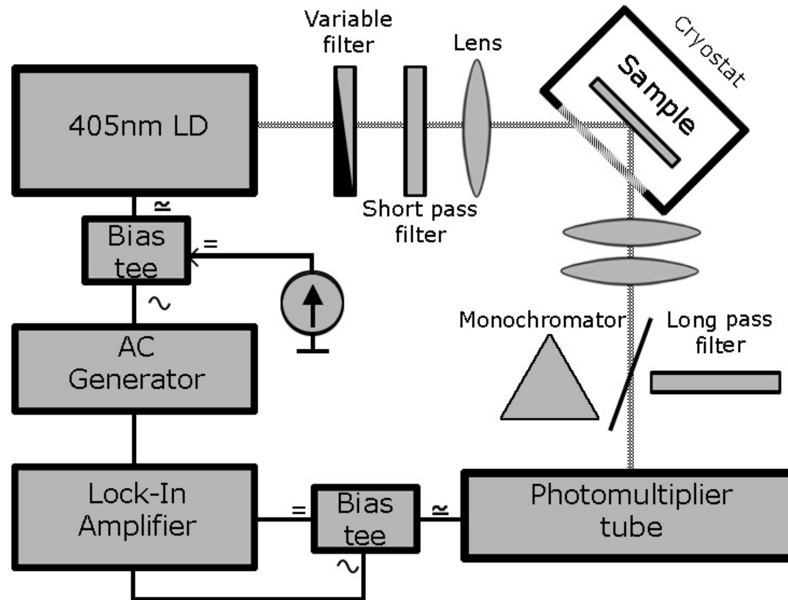

Figure 2.1 Experimental setup used for the frequency-domain measurements [P2].

The experimental setup is shown in figure 2.1. Two lock-in amplifiers enabled to cover the frequency range from 1 Hz to 100 kHz (SIGNAL RECOVERY 7265 DSP) and from 50 kHz to 100 MHz (STANFORD RESEARCH SYSTEMS SR844 with external modulator AEROFLEX IFR 2023A), resulting in a lifetime measurement dynamic range from 160 ms to 1.6 ns. A 405 nm LD was used as an excitation source in FDLM as well as for CW PL experiments, its excitation intensity was adjusted using a system of neutral gradient filter and a photodiode (OPHIR PD300-1W) to control an

excitation power. LD was electrically driven using a bias tee (PICOSECOND PULSE LABS 5547) ensuring the sum of DC current (to keep the LD in linear photo-respond versus current regime above lasing threshold) and a sinusoidal modulated AC signal. The samples were mounted in a

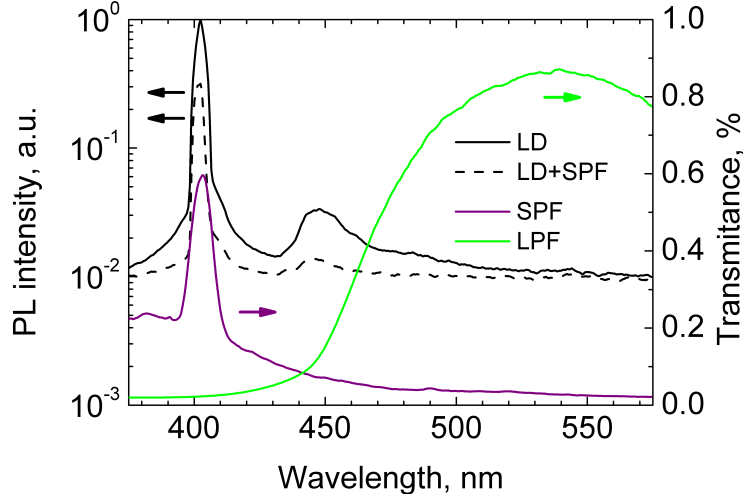

Figure 2.2 Normalized laser diode emission spectra with and without SPF (dashed and solid black lines, respectively). The transmission spectra of SPF (violet line) and LPF (green line) are also present [P2].

closed-cycle helium cryostat (CRYO INDUSTRIES 1644-GGS) to provide measurements down to 10 K. Light collected from a sample was focused onto a set of LPF (see Fig. 2.2) or to the entrance slit of a grating monochromator (JOBIN YVON H10 VIS), ensuring the best possible blockage of excitation light. The spectrally dispersed PL was detected using a PMT (HAMAMATSU H6780-01), connected to the lock-in amplifier. Phase shift

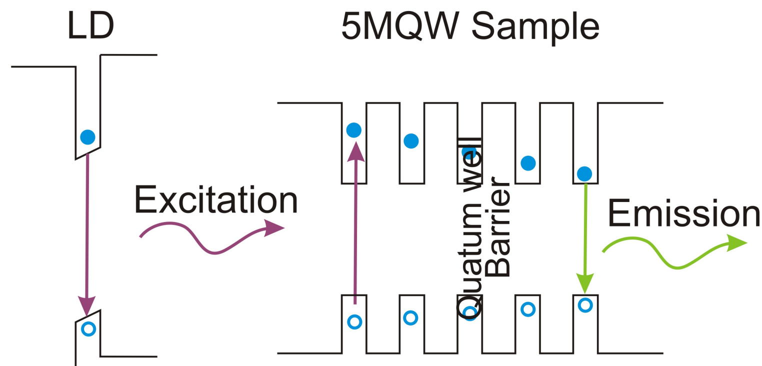

Figure 2.3 The scheme of optical resonant excitation [P2].

between LD modulation and PMT signals was measured as a function of LD modulation frequency. In order to obtain a background signal for establishing the reference phase shift of the experimental setup, the sample was replaced by a metal mirror and the set of LPF was removed (or the monochromator was set to the LD emission wavelength). It allowed to numerically eliminate the phase shift caused by the setup response. The carrier lifetime was extracted using Fourier-transformation analysis [33], the procedure is described in more detail in subsection 2.2.1. Such LD excitation wavelength was chosen so that the pump light is absorbed in the QWs only, while the barriers and the cladding layers remained unexcited (Fig. 2.3). The use of the LD as an excitation source allowed for carrying out experiments in a wide range of photoexcitation power densities, starting from 1 mW up to 15 W per square centimetre.

In order to further expand the excitation power density range, experiments in conventional TRPL setup were carried out. EKSPLA YAG:Nd3+ laser (pulse length of 30 ps and peak wavelenght of 355 nm) was used as an excitation source, while streak camera (HAMAMATSU STREAKSCOPE C10627) was used for signal registration.

2.2.1 Data processing

From a numerical point of view a system with a complex decay kinetic, consisting of three independent recombination channels, can be described by the common multi stretch-exponential decay formula:

$$I(t) = A_1 \cdot e^{(-\frac{t}{\tau_1})^{\beta_1}} + A_2 \cdot e^{(-\frac{t}{\tau_2})^{\beta_2}} + A_3 \cdot e^{(-\frac{t}{\tau_3})^{\beta_3}}, \quad (2.1)$$

here A_1, A_2 and A_3 are the intensity coefficients (pre-exponential factors), τ_1, τ_2 and τ_3 are the lifetimes, and β_1, β_2 and β_3 are the stretching parameters for each of the three exponential channels, respectively. In cases when any of stretching parameters $\beta_i \neq 1$, there is no analytical solution of Fourier transform of equation (2.1) and data points can not be fitted directly. However, the FFT of the function $I(t)$ gives real and imaginary parts in the frequency scale, which may be described as [34]:

$$\varphi_c(\omega) = \text{atan}\frac{Im(\omega)}{Re(\omega)}, \quad (2.2)$$

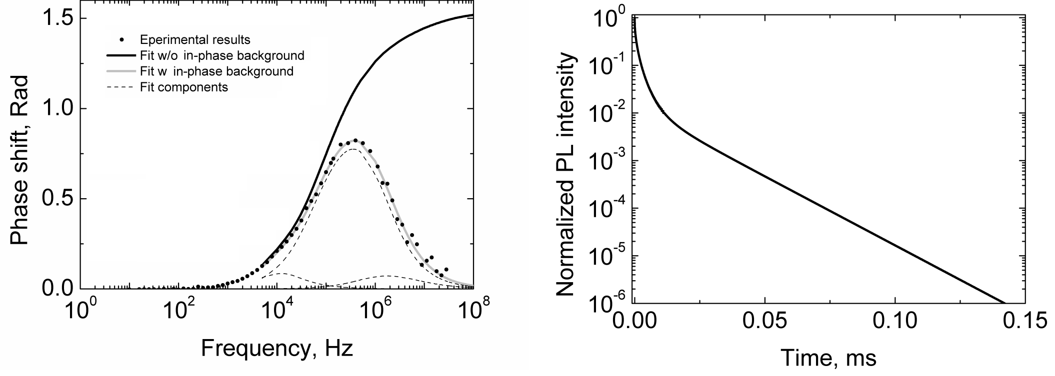

Figure 2.4 Left: comparison between experimental results (black dots) and calculated values with an in-phase background present (gray line, $\chi_R^2 = 3.5$) and without the in-phase background (black line, $\chi_R^2 = 860$), indicating high motivation to use Eq. (2.6) rather than Eq. (2.2). Dashed lines represent components of the gray line. Right: the time resolved PL curve, numerically obtained using Eq. (2.1) with the same parameters as those shown in the main plot [P2].

where $\varphi_c(\omega)$ is calculated phase shift and can be compared to one measured experimentally (between the reference and PL signals measured by the PMT), $Re(\omega)$ and $Im(\omega)$ are real and imaginary FFT transforms, respectively:

$$Im(\omega) = \frac{\int_0^\infty I(t) sin(\omega t) \mathrm{d}t}{\int_0^\infty I(t) \mathrm{d}t}, \tag{2.3}$$

$$Re(\omega) = \frac{\int_0^\infty I(t) cos(\omega t) \mathrm{d}t}{\int_0^\infty I(t) \mathrm{d}t}, \tag{2.4}$$

The use of FFT enables to change parameters in Eq.(2.1) until the sum of least squares between calculated phase shift obtained using Eq.(2.2) $\varphi_c(\omega)$ and experimentally measured results $\varphi(\omega)$ gives minimum value:

$$\chi_R^2 = \frac{1}{\nu} \sum_\omega \left[\frac{\varphi_c(\omega) - \varphi(\omega)}{\delta\varphi} \right]^2, \tag{2.5}$$

here ν represent the number of degrees of freedom (number of frequencies swept minus the number of variable parameters), $\delta\varphi$ is systematic uncertainty in the phase shift measurement. In cases when simple decay law is under investigation, one should expect χ_R^2 value near unity, while higher values indicate that more complex model should be involved or random noise is

affecting results significantly [34]. According to Lakowicz [34] if more complex model enables reducing χ_R^2 value twofold, it gives 99 % certainty that more complex model should be used to describe the experimental results.

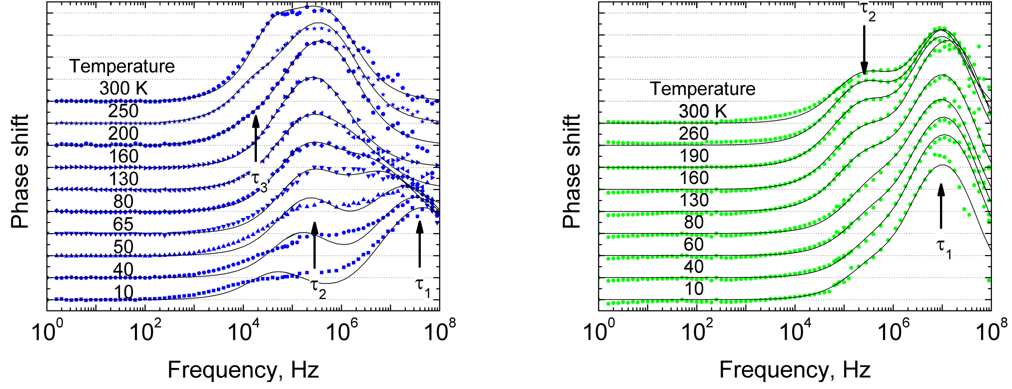

Figure 2.5 Comparison of FDLM experimental results (dots), measured using a 50 mW/cm2 excitation power density and fit (solid lines) using Eq. (2.6) as a function of the “blue” (left) and “green” (right) samples’ temperature. One major tick correspond to 10 Rad [P2].

In this study, the measured phase response curves showed shapes typical of a FDLM measurements with the presence of in-phase background, caused by the parasitic laser emission in blue spectral range and fitting results using Eq. (2.2) didn’t give acceptable χ_R^2 values (see Fig. 2.4). The presence of in-phase background was further confirmed by the fact that the influence of in-phase background was lower in the longer wavelength range as the parasitic PL gradualy decreases towards the longer wavelengths and was also increasing with the sample’s temperature as the PL signal of a sample decreased, while the intensity of laser’s parasitic emmision remained unchaged. In cases, when in-phase background is present and can’t be avoided, its influence can be numerically subtracted with measurable accuracy by adding a signal $S_{gnl}(\omega)$ to the in-phase background $B_{grnd}(\omega)$ amplitude ratio to the Eq. (2.2) [35]:

$$\varphi(\omega) = \operatorname{atan}\left(\frac{\frac{S_{gnl}(\omega)}{B_{grnd}(\omega)} \cdot Im(\omega)}{\frac{S_{gnl}(\omega)}{B_{grnd}(\omega)} \cdot Re(\omega) + 1}\right), \tag{2.6}$$

As the β is a parameter to evaluate system disorder [36] and excitation power densities or temperatures used in this study are too low to affect sample’s disorder, we presume β_1, β_2 and β_3 values to be constant for all

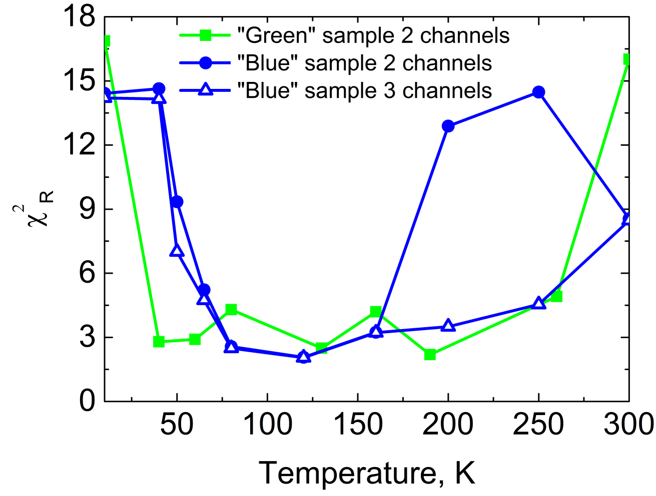

Figure 2.6 χ^2_R values obtained using the two-channel decay law for the "green" (green filled squares) and "blue" (blue filled dots) samples; the three-channel decay law for the "blue" sample (open triangles) gives a significant reduction of the χ^2_R value for temperatures of 200 K and 300 K. The lines are guides to the eye [P2].

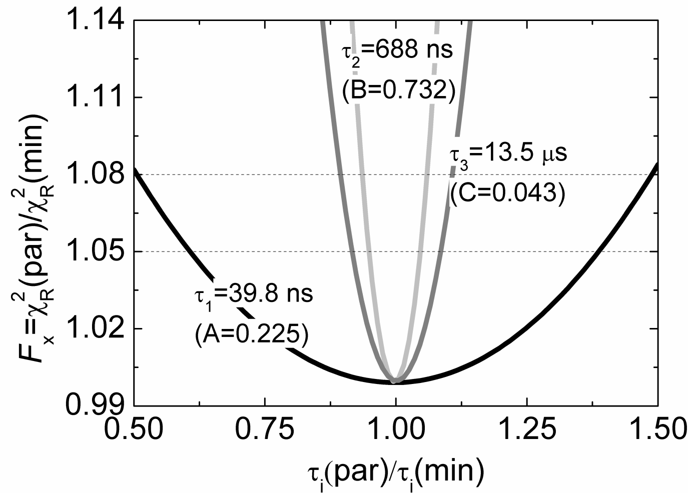

Figure 2.7 χ^2_R surfaces for τ_1 (black line), τ_2 (light gray line) and τ_3 (gray line) of "blue" sample, showing confidence intervals for two ($F_x = 1.05$) and three ($F_x = 1.08$) channels decay law [P2].

the measurements. We used temperatures where A_1, A_2 and A_3 coefficient values are as close as possible to fit β_1, β_2 and β_3 with lowest errors. Once the stretching parameters have been fitted, their values were kept constant, while other parameters (A_1, A_2, τ_1, τ_2 and τ_3, pre-exponential factor A_3 is described as $C = 1 - A - B$) kept variable in the rest of experiments, until the value of χ_R^2 reached a minimum.

Figure 2.5 shows comparison between experimental results (dots) measured using 50 mW/cm^2 excitation power density and least square fit (solid lines represent FFT of Eq. (2.1) using Eq. (2.6) to relate calculated $\varphi_c(\omega)$ and measured $\varphi(\omega)$ values) for the "blue" and "green" samples respectively. Figure 2.6 represents χ_R^2 as a function of temperature. It is clearly seen that there is at least threefold reduction of χ_R^2 value while switching from 2 to 3 channel decay model for blue sample at temperatures of 200 K and 250 K.

Confidence intervals for each parameter can be evaluated by calculating χ_R^2 surfaces [34]:

$$F_x = \frac{\chi_R^2(\mathrm{par})}{\chi_R^2(\mathrm{min})} = 1 + \frac{p_a}{\nu} \cdot F(p_a, \nu, P), \tag{2.7}$$

here $\chi_R^2(\mathrm{par})$ represents value of χ_R^2 with one of parameters value set at a value different from that yielding the minimum value of $\chi_R^2(\mathrm{min})$, p_a is number of parameters, $F(p_a, \nu, P)$ is a value from Fisher's F Statistic Table [37] with p_a parameters and ν degrees of freedom with a probability of P. F_x value of 1.046 gives 68 % probability that parameter value is consistant with experimental result in case of two exponential decay law, while in the case of three exponential decays $F_x = 1.078$ should be used to get same probability [37]. For ease of data interpretation we used F_x values of 1.05 and 1.08, for two and three channel decays respectively. Three χ_R^2 surfaces are ploted in figure 2.7 (obtained for "blue" sample using 50 mW/cm^2 excitation power density at 250 K temperature) to give a visualization of confidence interval values in the case of two and three channel decays, as well as their dependences on pre-exponential factors. Confidence intervals are also shown in figures, represented in subsection 2.3.1.

2.3 Experimental results

2.3.1 Temperature dependency

Temperature dependence study was performed, as it provides good insight of radiative and non-radiative recombination mechanisms in InGaN/GaN LED structures. To explain the results a well-adopted model of a charge carrier localization at a different confining potential and thermal activation featuring PL spectra peak energy S-shaped shift temperature dependancy was used [38, 39]. Starting from low temperature, carriers are randomly distributed among the potential minima (see Fig. 2.8a). As the tempera-

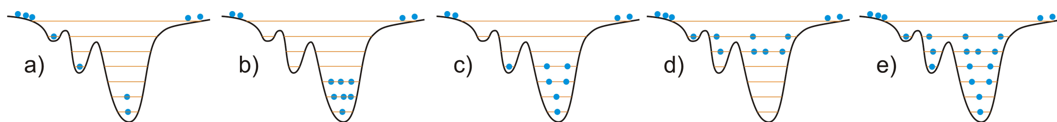

Figure 2.8 Schematic diagrams of carrier redistribution in a MQW structure depending on the temperature as proposed by Wang and co-workers [39] (a)-(d) and photoexcitation affected carrier delocalization (e) [P2].

ture increases, weakly localized carriers are thermally activated and relax down into other strongly localized states via hopping and reach a saturated redistribution (Fig. 2.8b) [40, 41, 42]. This leads to carrier lifetime increase, giving the carriers more opportunity to relax down into a lower energy tail states caused by the inhomogeneous potential fluctuations. This effect was observed for both, "blue" and "green", structures at low excitation power densities and temperatures between 50 and 100 K. A rapid increase of the carrier lifetime up to around 25 ns for the "blue" structure (Fig. 2.9c) and up to 60 ns for the "green" structure (Fig. 2.10b) with increasing temperature was observed. The dominance of these relative fast decay components was secured by their high pre-exponential factors (Figs. 2.9d, 2.10c). Then, following the pre-exponential factor and the domination of the decay times in the sub-microsecond range, a prolonged increase of the decay time with temperature up to around 1.5 μs at a 150 K for both structures was observed, which is best viewed at the lowest photoexcitation power density (Figs. 2.9b, 2.10a). This feature, however, was quenched at higher photoexcitation. The increased photoexcitation and re-distribution by temperature simultaneously made the carriers undergo a markedly bandfilling process

in the lower levels of localized states ending up with delocalization towards defect related sites with non-radiative recombination (e.g., point or interface defects, threading dislocations) or to a deeper recombination channels with even longer decay times (T $>$ 170 K [43, 44]) (see Fig. 2.8c,d). According to the literature non-radiative process starts to be dominant above 150 K, in this case the decay times are in a sub-microsecond, for the "blue" structure, and in a nanosecond, for the "green" structure, range (Figs. 2.9d, 2.10c) [43].

Extreme long lasting localization sites, in particular for the "blue" structure, were expressed by a very long lifetimes (Fig. 2.9a) reaching 15-25 μs (at 200 K) with their pre-exponential factors gradually increasing up to 20 % at room temperature (Fig. 2.9d).

The model used to interpret the temperature dependencies of channel's inputs in the decay law is schematically described in figure 2.11. Competition of a radiative (1) and several non-radiative (2-4) recombination channels was analyzed, as a common practice for InGaN/GaN MQW structures [38]. According to the experimental results for the "blue" structure presented in figure 2.9d the fast radiative recombination channel's intensity coefficient decreases with increasing temperature due to an activation of carriers from the channel 1, these carriers redistribute to channel 2 (pre-exponential factor of the channel 2 gradually increases). At temperatures higher than 200 K carriers have enough energy to be redistributed to the channel 3 as well. Initial decrease of fast recombination pre-exponential factor up to 150 K for the "green" structure (Fig. 2.10c) can be explained in the same way. Differently from the "blue" structure, here is further decrease of intensity coefficient of ns radiative channel 1 with a temperature is compensated by the increase of fast ns non-radiative channel's 4 pre-exponential factor (curve is not decomposed in Fig. 2.10c). Moreover, absence of channel 3 and weak influence of channel 2 suggest the channel's 4 high capacitance to drain carriers, for the "green" structure. The addition of channel 4 to the green structure is also suggested by lower sample's IQE value. For both analysed samples a substantial change on the impact of recombination channel with increasing photoexcitation power density is observed. This trend may result from carrier diffusivity enhancement discussed in the subsection 2.3.2. Finally, at a room temperature we end-up with slightly different picture on the carrier dynamics for the two structures

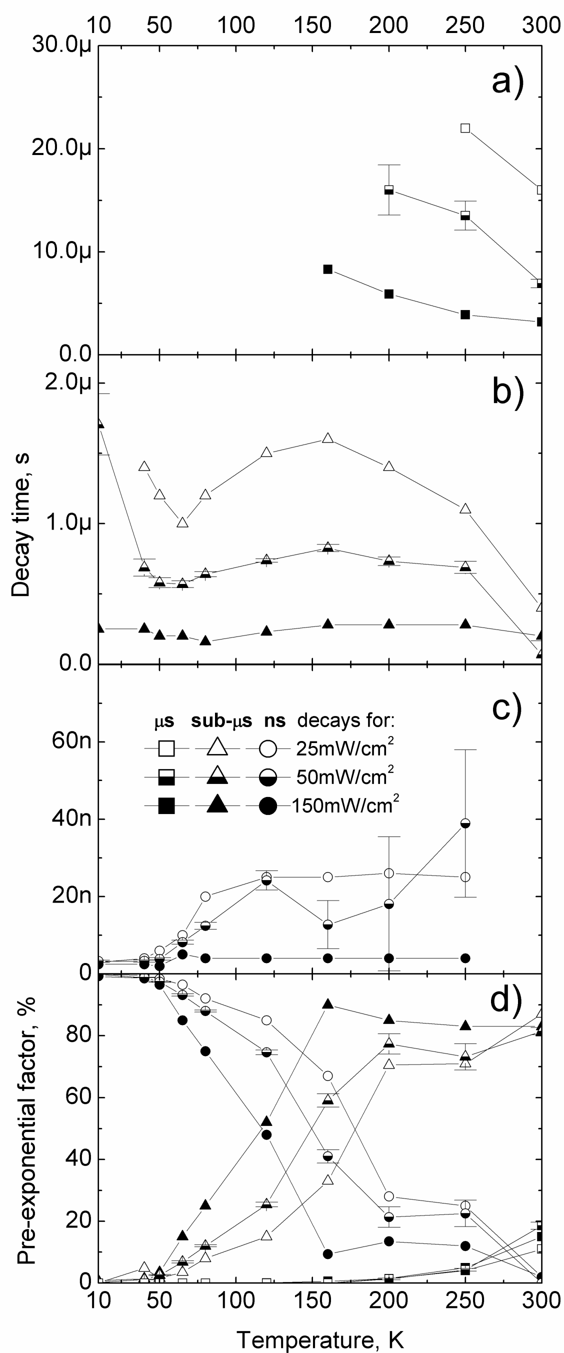

Figure 2.9 PL decay time (τ_1 (c), τ_2 (b), τ_3 (a)) and pre-exponential factor A_1 (circles), A_2 (triangles), A_3 (squares) (d) for the nanosecond (c), sub-microsecond (b), microsecond (a) time range, respectively, as a function of temperature, using photoexcitation power density of 25 (open), 50 (half filled) and 150 mW/cm^2 (filled) for the "blue" LED structure. Error bars are evaluated according to procedure described in subsection 2.2.1 and are shown only for 50 mW/cm^2 excitation power density. The lines are guides to the eye [P2].

investigated. The recombination process for the “blue” structure is led by a non-radiative channel with sub-microsecond range lifetimes, supported by a channel of even slower microsecond decay time. The “green” structure instead manifests a higher density of defects related fast nanosecond non-radiative recombination channels sharing the pre-exponential factor from a localized states of sub-microsecond lifetimes by 97 % and 3 % (for lowest photoexcitation power density), respectively. Higher In composition for the “green” structure may imply deeper localization, effects such as larger internal field or defects assisted tunnelling (due to higher density of point defects can lower the barrier for emission from the localization centers) resulting in more rapid decrease of lifetimes as proposed by Minsky *et al.* [44].

The PL decay analysis revealed a rather stretched exponential behavior for most of the decay times. The stretched exponential decay is consistent with significant disorder in the structure. The extracted values of a stretching parameter for the “blue” structure are 0.49±0.02, 0.61±0.01 and 1±0.02 for the nanosecond (Fig. 2.9c), sub-microsecond (Fig. 2.9b) and microsecond (Fig. 2.9a) decay time range, respectively, while for the “green” structure, values are 0.91±0.03 and 0.59±0.02 for the nanosecond (Fig. 2.10b) and sub-microsecond (Fig. 2.10a) decay time range, respectively, confirming the relative disorder. The stretching parameters for the nanosecond and sub-microsecond decay time range in the case of the “blue” structure and for the sub-microsecond decay time range in the case of the “green” structure corresponded well to those obtained using TRPL, 0.47 and 0.54 for the “blue” and “green” structures, respectively (stretching parameter evaluation procedure is described in more detail in subsection 2.3.2 and Ref. [36]). These values are comparable with those published by Pophristic and his co-workers, who used a TRPL to investigate LED structures emitting in the blue spectral range and obtained stretched exponential lifetimes spreading from 500 ps to 3 ns with a stretching parameter of 0.59±0.05 [36]. This implies that stretching behaviour of the samples investigated can also be attributed to an indium phase segregation and the associated spatial fluctuations of the local indium concentration in the well, as proposed by Pophristic *et al* [36]. In the TRPL experiments ultrashort laser pulses and, consequently, relatively high photoexcitation power density was used, though the stretching parameter value remained relatively stable. Using FDLM the author have managed to supplement this high photoexcitation power density result sig-

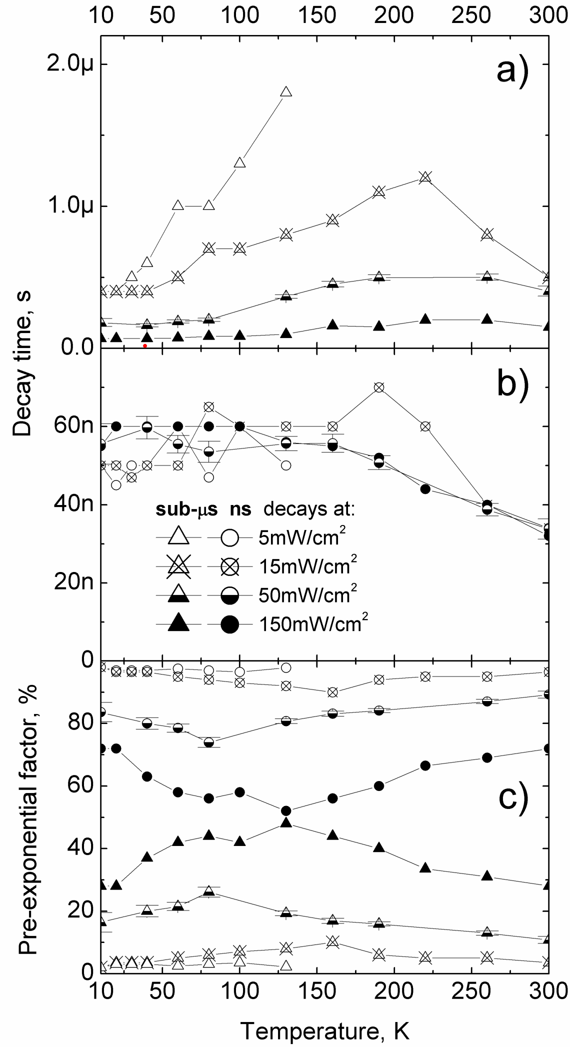

Figure 2.10 PL decay time (τ_2 (b), τ_1 (a)) and pre-exponential factor A_1 (circles), A_2 (triangles) (c) for the nanosecond (b), sub-microsecond (a) time range, respectively, as a function of temperature, using photoexcitation power density of 5 (open), 15 (crossed), 50 (half filled) and 150 mW/cm^2 (filled) LD photoexcitation power density for the "green" LED structure. Error bars are evaluated according to procedure described in subsection 2.2.1 and are shown only for 50 mW/cm^2 excitation power density. The lines are guides to the eye [P2].

nificantly by covering a wide excitation power density range. It allowed to obtain stretched exponential lifetimes from 2-4 ns up to about 1.5 μs with the same stretching parameter.

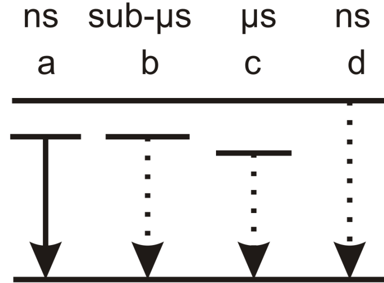

Figure 2.11 Schematic diagram of the suggested recombination model. A solid arrow represents radiative while dashed ones corresponds to non-radiative recombination channels [P2].

The nearly exponential decay in the nanosecond range obtained by the FDLM for the "green" structure is reasonable due to a higher indium content in its QWs therefore higher localization should be observed. Similarly, the microsecond single exponential decay time for the "blue" structure with a substantial pre-exponential factor at room temperature indicates a characteristic long lasting carrier localization site (Fig. 2.9d).

Decay channels' activation energies were extracted and the dependencies on the photoexcitation power density have been drawn (see Fig. 2.12). It appeared that the activation energy values are in the range of 20÷40 meV for all the time ranges and for both structures are much less than the band offsets as well as the band-gap difference between the wells and the barriers; therefore one could conclude that the thermal quenching of the PL emission is not due to the thermal activation of charge carriers from the InGaN QWs into the GaN barriers. Instead, the dominant mechanism leading to the quenching of the InGaN-related PL may have several explanations: (i) the thermionic emission of the nonequilibrium carriers out of the potential minima caused by the band potential fluctuations due to the composition, well width and interface fluctuations [43, 44], (ii) higher local temperature facilitated tunneling process typically assisted by acoustic phonons [45]. The decrease of the activation energy with photoexcitation power density appeared to be in-line with the delocalization effect observed and analyzed by Wang and co-workers in InGaN/GaN MQW structures [39]. In our case, despite the somehow tangled dependencies, still lower activation energy

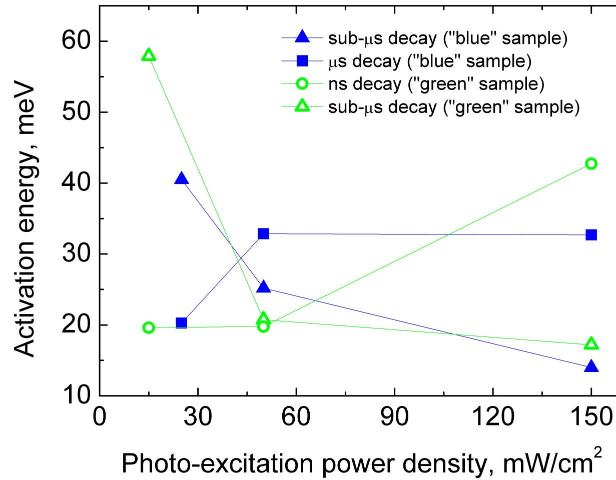

Figure 2.12 Activation energy of the PL decay channel τ_2 for the sub-microsecond (filled triangles), τ_3 for the microsecond time range (filled squares) and τ_1 for the nanosecond (open circle), τ_2 for the sub-microsecond time range (open triangles) as functions of photoexcitation power density for the "blue" (filled) and "green" (open) LED structures, respectively (symbols according to Figs. 2.9 and 2.10). The lines are guides to the eye [P2].

values could be attributed to the "blue" structures supporting the above interpretation about more effective delocalization.

2.3.2 Photo-excitation power density dependency

To reveal in more details the carrier recombination dynamics, investigation of the decay dependency on photoexcitation power density was performed. In figure 2.13, the dominant decay time values in the kinetics at room temperature for both "blue" and "green" structures are presented. Here, a further development of the situation with quenching of non-radiative recombination channels and delocalization enhancement can be seen. A general trend toward decrease of the carrier lifetimes with increasing photoexcitation is seen for both structures, even more pronounced for the "blue" one. Basically, the decay components have a trend that the faster the decay time is the higher its intensity coefficient is (not presented). For example, the "green" structure has a fast dominant component at low excitation power density, while with increasing excitation density both components are merging (pre-exponential factor become comparable). For the "blue"

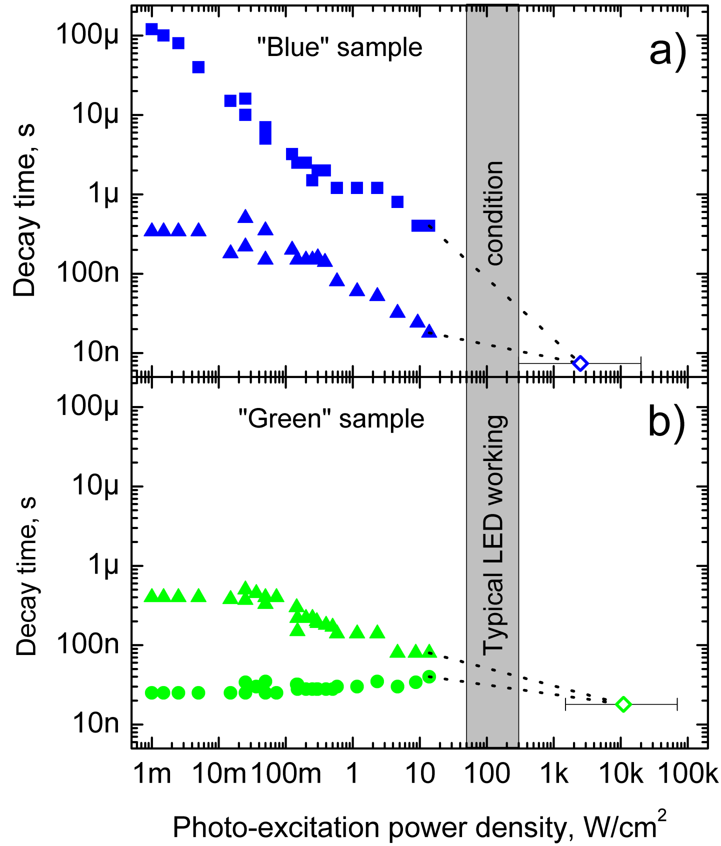

Figure 2.13 PL decay time (τ_2 (full triangles), τ_3 (full squares)) (a) of the "blue" LED structure (no input from the nanosecond range as the pre-exponential factor at the room temperature is negligible, as seen from Fig. 2.10d) and PL decay time (τ_1 (full circles), τ_2 (full triangles)) (b) of the "green" LED structure as functions of LD photoexcitation power density at 300 K temperature. Cross represents PL decay time (τ_1) of the "green" LED structure under LED photoexcitation at 300 K temperature. Open diamonds represent decay times of the conventional TRPL kinetics of the "blue" and "green" LED structures from figure 2.14 and extracted via figure 2.15. The horizontal bars represent the photoexcitation power density uncertainty due to a fact that pulsed excitation was used. Gray shaded area represents power density of a typical working LED [P2].

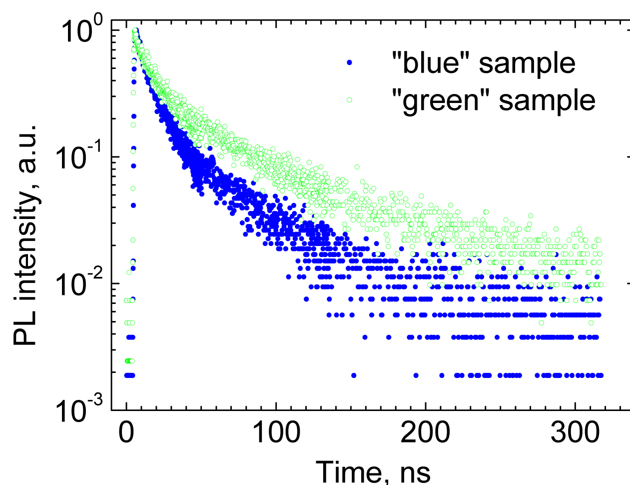

Figure 2.14 TRPL kinetics of the "blue" (full circles) and "green" (open circles) LED structure at 100 mW/cm^2 LD photoexcitation power density measured at room temperature [P2].

structure, as the time decay are widely apart the faster one dominates in the whole excitation power density range. It was shown that with increasing photo-excited carrier concentration their diffusivity increases [46]. This enables carriers to reach more distant localization centers and enhance either non-radiative or radiative recombination resulting into a lifetime decrease (Fig. 2.8e). The photoexcitation affected delocalization in our case is more expressed for the "blue" structure (rapid decay time reduction versus photoexcitation). The "green" structure, however, demonstrates shorter and almost constant decay time versus photoexcitation power density due to higher non-radiative center density and their saturation is not reached. This is consistent with the temperature dependencies discussed above. The observed trend was supported by the TRPL measurements providing decay times (7.4 ns and 18 ns for "blue" and "green" structures, respectively) far away on the photoexcitation power density scale (see diamonds in Figs. 2.13a,b and Figs. 2.14, 2.15). These values comply with the TRPL results published in a literature on blue emitting MQW structures (1.5-2.5 ns and 24-42 ns, 8 MW/cm^2 [46]) confirming the tendency shown by a dashed line in the figure 2.13 and verify the idea about effective delocalization of carriers in the "blue" structure and still relative high concentration of unsaturated recombination centres for the "green" structure.

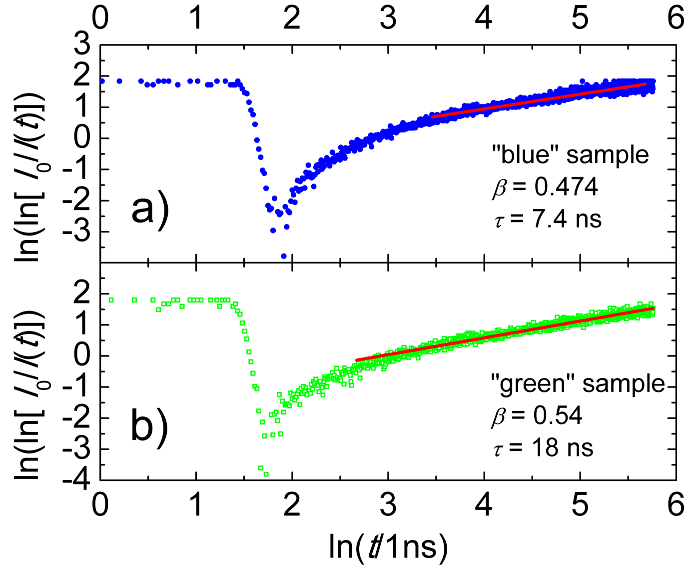

Figure 2.15 The TRPL kinetics of the "blue" (a) and "green" (b) LED structure (from Fig. 2.14) plotted by $\ln(\ln[I_0/I(t)])$ vs logarithm of time t used to determine β and τ (see the legend). The slope of the red line equals to β, while the intercept is $-\beta \cdot \ln \tau$ [36]. The extracted decay times (marked as open diamonds) are presented in figure 2.13 [P2].

2.4 Conclusions

A wide range of excitation power densities provided by a laser diode significantly broadens the capabilities of the frequency domain lifetime measurement technique for optoelectronic device investigation. InGaN MQW LED test structures, that emit in blue and green spectral range, revealed several recombination channels with characteristic nanosecond, sub-microsecond and microsecond decay times, when investigated with this extended technique. Stretching character of the multi-exponential decays was disclosed and corresponding parameters were evaluated revealing LEDs wafers' structural disorder.

3. Semi-planar III-nitride LED fabrication method by femtosecond ablation

3.1 Introduction

45 years have already passed since the first device, based on GaN, EL was demonstrated [47]. However, at that time it was a low efficiency metal-insulator-semiconductor device, as *p*-doped GaN was not yet been available. Conventional *p*-*n* junction LEDs have become possible only after Amano *et al.* have managed to grow *p*-type GaN epitaxial layer by MOCVD method [48]. However there were no good etching solutions for the GaN at that time [49], so first LED [48] has been realised using out-of-the-box approach by forming *n*-type contact on a side wall of LED chip. Only after adopting the reactive ion etching technology by Nakamura *et al.* [50] full commercialisation of GaN based LED become possible. Despite the n ew tendencies in GaN devices' production, e.g. developement of photoeletrochemical etching approaches [51], vertically structured LEDs made by laser lift-off process [52], non-polar or semi-polar epitaxial growth [53], tunnel junction LEDs [54], flip-chip [55], quatum dot [56] or nanorod [57] LEDs, nearly all commercially available LEDs are still produced basing on the principles first laid by Amano and Nakamura. Most of LEDs still are using MQWs based active region, while being grown on c-plane sapphire (0001) crystal orientation, wafers are then separated into dies and *n*-type GaN is being exposed via dry chlorine based etching. Until recently there seemed to be little possibilities for GaN based device fabrication in Lithuania. Few notable attempts are the first batch of LEDs produced by dr. T. Grinys [N5] in laboratories of prof. C.C. Yang (Graduate Institute of Photonics and Optoelectronics National Taiwan University, Taipei, Taiwan), also dr. I. Kašalynas fabrication of high electron mobility transistor [58] at prof. M. Leszczynski laboratory (Institute of High Pressure Physics UNIPRESS, Warsaw, Poland). Until the opening of National Centre of Physical and Technological Sciences in

Vilnius in spring 2016, there were almost no possibilities to produce working GaN devices in Lithuania due to the fact that all technological instruments weren't available at all or were diluted within a number of different institutions in Vilnius. At that point it seemed very attractive to fill up these technological gaps and overcome the difficulties by adapting and employing the biggest high tech industry existing in Lithuania - laser manufacturing.

It is well known that femtosecond pulse ablation produces neither melting, nor craters of melted material around ablated area, contrarily to the ablation with nano or picosecond pulses [59, 60, 61]. The melting process occurs due to photo excited electron cooling and lattice heating. The characteristic time for the electron cooling is less than 1 ps, for the lattice heating hundreds of picoseconds [60]. Therefore, the ablation with femtosecond pulses provides almost no heat transfer to the lattice [59, 62]. Various types of surface structures at nano- and micro-scales on metals and semiconductors have been created providing highly absorptive matter [63]. Benefits and capabilities provided by femtosecond lasers are very attractive also for the gallium nitride ivestigators' community. The number of fs laser applications to GaN grows every year. First applications were involved in charge carrier lifetime measurements in GaN [64, 65, 66]. Just after, the first femtosecond laser machining attempts appeared trying to make trenches in GaN [67, 68], as a useful method for chip separation. Lots of work has been done using the femtosecond laser machining to increase light extraction from LED by texturing GaN [69] or its substrate [70, 71, 72], some of the publications demonstrate novel approaches, such as photonic crystal [73] or Fresnel lens [74] structures. There is a new growing group of publications showing femtosecond laser as a direct writing tool for photoresist exposure on various materials [75], including GaN [76]. Despite the fact that this approach avoids producing expensive photoresist masks for a small batch prototyping, it still fails to provide a faster or cheaper process. Rapid resistless prototyping and substitution of processing steps in conventional optoelectronic device manufacturing by laser direct writing techniques is a very attractive way to gain effectiveness of production time and costs. Three years ago an impressive progress has been demonstrated in laser manufacturing of thin film solar cells by using ps laser pulses [77]. However, until recently [P3], it seemed there were no publications about fs laser as a direct writing tool for GaN device processing, mainly due to the

fact that extremely accurate ablation depth control and surface morphology of the bottom part of the mesa is needed. Fast processing of GaN LEDs using ps laser was proposed by Moser and co-workers [78, 79]. However, due to the above mentioned advantages, more accurate results could be obtained by using fs laser pulses. The application of fs processing in LED production is a very urgent industry driven challenge. Therefore, development and implementation of new approaches may be crucial for prototype and small-volume production LED manufacturers.

The author's extension of a well-known Amano LED *n*-contact-on-a-sidewall approach [48] led to an unexpected discovery of simple, rapid and accurate LEDs processing method using ultrashort laser pulse ablation in a 45° geometry. It allowed reducing the number of fundamental processes and critical alignment steps, resulting in a reduced LED fabrication duration.

3.2 Experimental setup

The principal scheme of laser-processing system is shown in figure 3.1. A single-unit integrated Yb:KGW femtosecond laser ("PHAROS" of LIGHT CONVERSION) was used for laser-processing (1030 nm, 320 fs, 20 kHz - 1 MHz). The maximum pulse energy was 0.4 mJ and maximum output power 6 W depended on repetition rate. A set of a half-wavelength plate and a thin-film polarizer were used as an attenuator to reduce pulse energy from its maximum value. The resulting beam quality factor M^2 of the laser output was better than 1.2. The high resolution and repeatability five axes motorized system (AEROTECH, X and Y - ANT180-160-L-ES17401, Z - ANT130-060-L-ES17401, R1 - ANT130-360-R-ES17401, R2 - ADRS-150-ES17401) was used for sample translation. The accuracy of the X-Y stages was ±150 nm and ±2 μm for Z stage. The resolution was 1 nm for all (X-Y and Z) stages. The accuracy of the rotation stages was 10 and 80 arcsec, resolution 0.01 and 6.5 arcsec for R1 and R2 rotation stages respectively. A vacuum sample holder was mounted on a platform of rotation stage R2. The CMOS camera (MVBLUEFOX 102C) was used for *in-situ* ablation process observation, under illumination of 660 nm peak wavelength LED.

3.2.1 Masks fabrication

The 30 μm thick 99.9 % pure molybdenum foil was used to fabricate masks (see Fig. 3.2) for LED contacts formation and mesa etching. The molybdenum was chosen as a mask material because of its high melting temperature (2617°C) and low thermal expansion coefficient (4.8 μm·m^{-1}·K^{-1} at 25°C) [80]. The foil was glued on the glass substrate and mounted on a vacuum chunk fixed to the R2 rotational stage. The glue kept the foil flat and didn't allow bending during the ablation process. An aspheric lens (F = 4.03 mm, NA = 0.62) was used to focus the laser beam perpendicular to the foil surface. After each circle of the ablation the lens was lowered to the surface according the ablation depth (d=3 μm). 10 ablating steps were chosen to complete the foil ablation through the entire thickness. The translation speed was 2 mm/s, the laser pulse energy and repetition rate was 1.2 μJ and 25 kHz, respectively. This resulted in 8.4 μm wide ablation trench as measured *ex-situ* by SEM (see Fig. 3.3). After the ablation process the glue was dissolved and the mask was cleaned with distilled water.

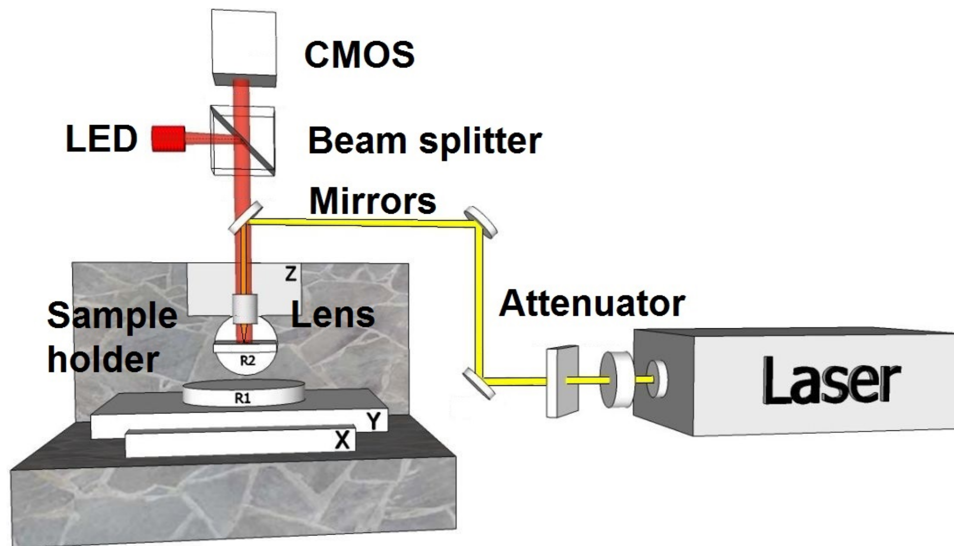

Figure 3.1 The molybdenum mask formation scheme using Yb:KGW fs laser. The setup utilizes a vertical (Z) and two horizontal (X, Y) translation and two rotational (R1, R2) stages. A vacuum sample holder is mounted on the rotational stage R2 [P3].

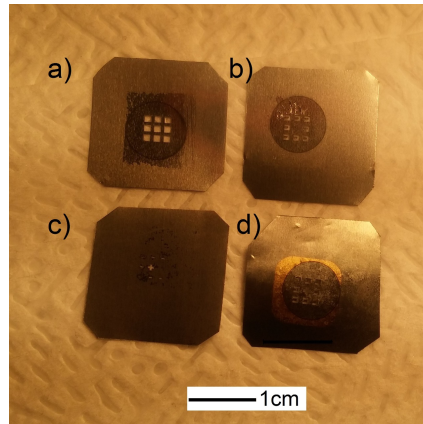

Figure 3.2 Molybdenum masks used for LED fabrication process: (a) for chip mesa formation, (b) for *p*-mesa etching, while (c) and (d) masks were used for contact formation (the only two masks used in the case of laser LED). Darker metal artefacts visible on the masks are residues due to the chromium sputtering on sapphire using custom build shadow mask holder.

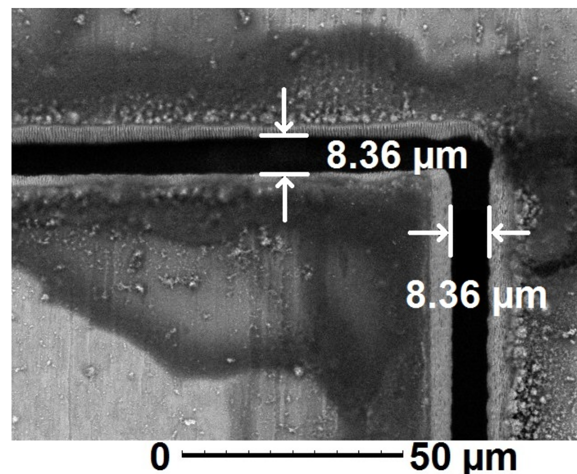

Figure 3.3 SEM image of a molybdenum mask illustrating the ablation profile.

3.2.2 Devices processing

The fabrication of a conventional LED consists of four fundamental process steps, as follows:

1. creation of *p*-mesa structure by dry RIE etching the *p*-type GaN down to the *n*-GaN for deposition of the ohmic *n*-contacts (see Fig. 3.4b);

2. wafer separation into individual LED dies by dry etching trenches down to the undoped GaN epi-layer (see Fig. 3.4c);

3. deposition of ohmic metal contacts onto the *p*-GaN (see Fig. 3.4d);

4. evaporation of ohmic contacts onto the exposed *n*-type GaN areas (see Fig. 3.4e).

All of these steps also includes spin-coating photoresist layer on top of the sample, mask alignment (in this case mask was chromium on sapphire substrate, that was made using Mo foil as shadow mask, as described further in this subsection), photoresist exposure, development and finally stripping the residual resist layer.

In the case of direct 45° angle laser ablation process, the chip separation trenches and the *n*-GaN layer exposure is being made simultaneously. Thus, this approach reduces the fundamental process steps by one (see Fig. 3.4 f-i). Therefore, the number of critical alignment steps is reduced and overall process time is shortened.

In order to make trenches and *n*-GaN exposure, the GaN wafer was put on a rotation stage providing a laser beam incidence angle of 45° (Fig. 3.5). The angle was chosen so in order to provide still an appropriate base of the exposed *n*-GaN. An increase of the angle would steepen the slope, making it difficult if possible to form an *n*-type contact. Angle decrease would excessively increase the device spacing and significantly reduces the number of produced devices per area. In the case of GaN ablation, an aspheric lens (F=16 mm and NA=0.16) was used to focus the laser beam to the sample. During GaN ablation the scanning speed was set to 0.5 mm/s, what resulted into an inter-pulse distance of 20 nm. The process pulse energy was gradually reduced until 1 μJ, no damage to the plain sapphire layer was observed using in-situ CMOS monitoring system (Fig. 3.5). To secure the undamaged ablation regime (so-called self-limiting regime [79])

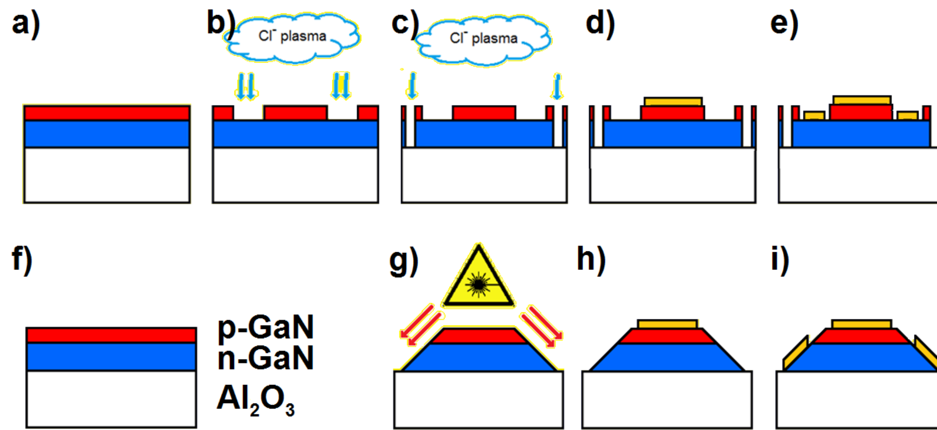

Figure 3.4 Processing sequence for conventional LED using approach (photolithography and RIE dry etching) a-e and sequence to produce LEDs using inclined laser ablation. Red layer represents *p*-type GaN, blue is *n*-type GaN, while sapphire is marked as a white square, yellow shapes represents a metal contacts. a) as grown b) *n*-GaN exposure by Cl_2 plasma etching c) chip separation trenches formation by deep Cl_2 plasma etching d) *p*-contact formation e) finished LED chip after *n*-contact evaporation; f) as grown g) chip separation and *n*-GaN exposure by fs laser ablation h) *p*-contact formation i) *n*-contact evaporation on *n*-GaN layer sidewalls [P3].

the energy was additionally reduced by 10 %. *Ex-situ* observed by SEM the GaN ablation trench was 8 μm wide, resulting to an ablation energy of 0.9 μJ (fluence was 0.45 J/cm^2).

During the ablation in air the formation of an oxide layer (see Fig. 3.6a) cannot be suppressed. Since sapphire was not damaged while ablating the GaN, the oxide film consisted entirely from GaO. 0.5 % KOH treatment was applied in order to remove the GaO (see Fig. 3.6b) layer before metallization process, which otherwise might reduce parasitic parallel and/or increase parasitic serial resistance of the LED [81]. Another option is to perform ablation in a noble gas ambience, which would prevent formation of GaO layer. In figure 3.6c it is visible that ablated inclined side wall region lacks for N, however, on the side wall there is no evidence of Al or O. The lack of N implies that GaN layer decomposed into gaseous nitrogen and metal gallium droplets, that are easier to remove by various solvents in comparison to the GaO layer. After the sample is cleaned from the ablation residuals, a contact evaporation process can be arranged.

In order to get more comparable results between conventional and laser

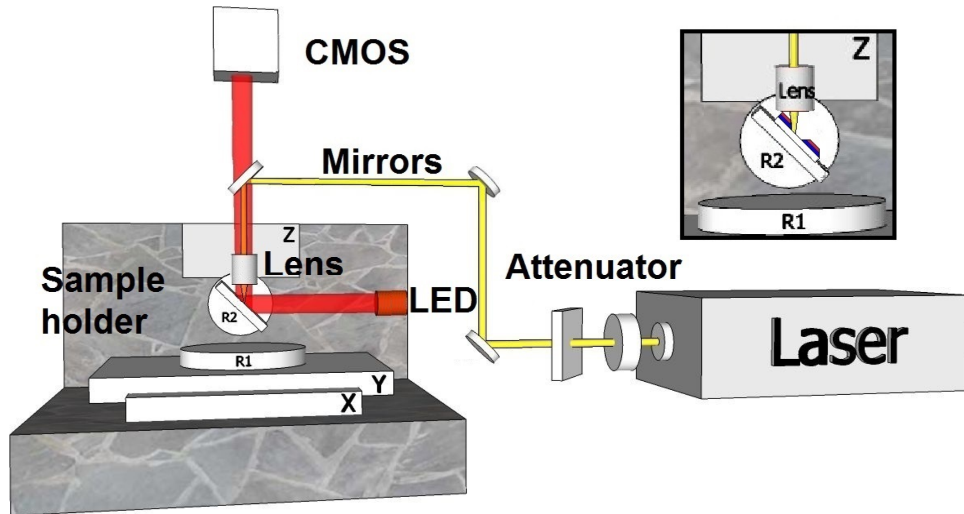

Figure 3.5 The GaN trench formation scheme, tilted by for 45° angle. The setup utilizes a vertical (Z) and two horizontal (X, Y) translation and two rotational (R1, R2) stages. An inset shows the sample fixed on the inclined rotational stage R2 [P3], without the red LED illumination for the *in-situ* ablation monitoring, which is shown in the main plot.

ablated LEDs the molybdenum foil with shadow mask pattern was put on a custom build shadow mask holder/aligner and 200 nm chromium layer was sputtered (QUORUM, Q150T) on a plain sapphire substrate through the openings in the mask. The substrate with chromium patterns was then used as a standard photolithography mask to expose photoresist for the deposition of *p*- and *n*-type contacts on GaN layers or to form LED's mesas via dry etching.

This was done only in order to make the laser sample's contacts under same conditions as for the reference sample. It is important to point out that the contact metals could have been deposited directly on GaN through the openings in a molybdenum foil using the same custom build shadow mask holder/aligner. The reference sample processed using conventional fabrication steps (see Fig. 3.4c) and LED made in a 45° ablation geometry (see Fig. 3.4g) were then covered with a photoresist and exposed using chromium on sapphire mask and developed. Both samples were simultaneously put into an electron beam evaporator (ULVAC EB EO184) for the deposition of the ohmic *p*-contact (20 nm Ni / 80 nm Au). After the lift-off process the procedure was repeated with another mask for *n*-type contact deposition consisting of 20 nm Ti covered by 200 nm Au layer. This resulted

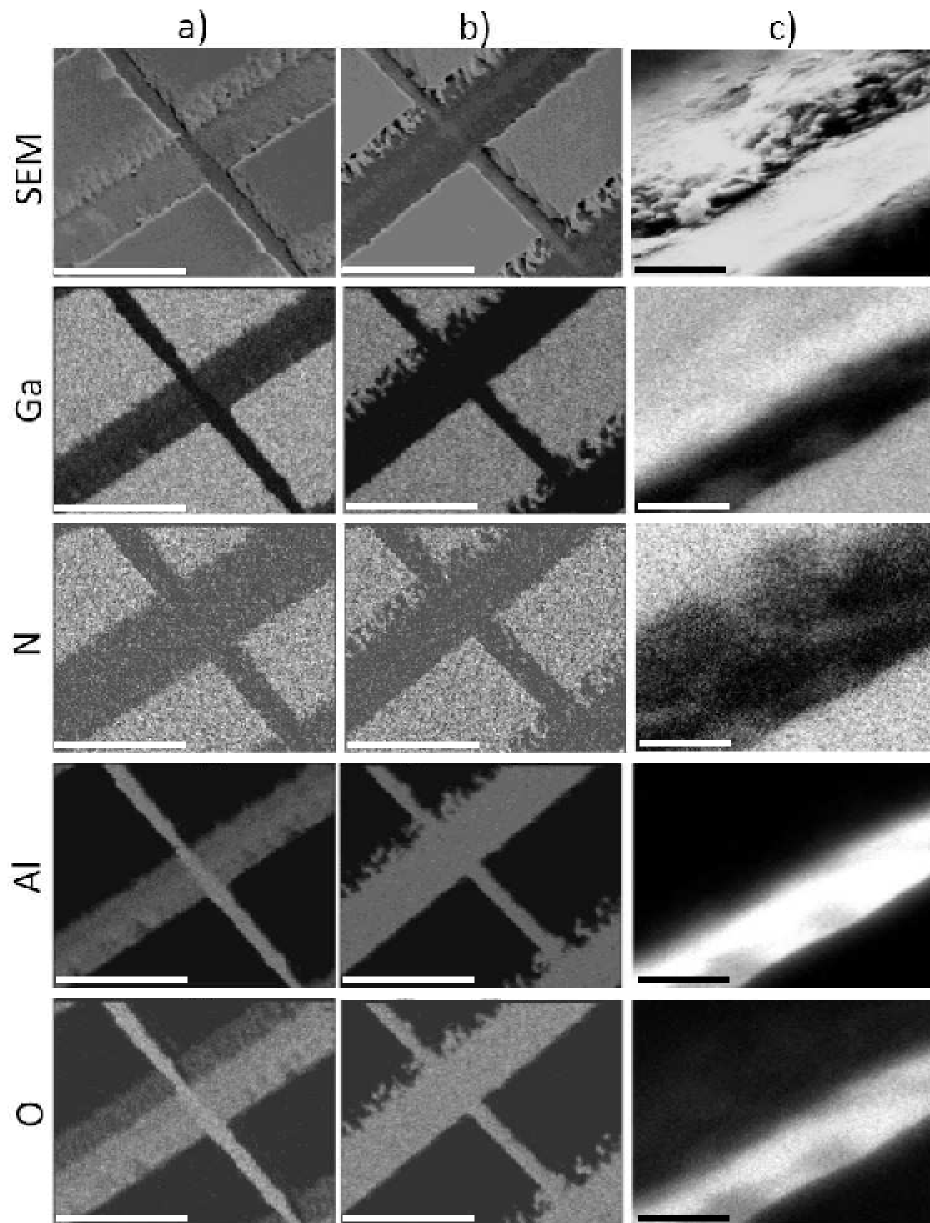

Figure 3.6 Top to bottom: sample's SEM image and elemental maps for Ga, N, Al and O, acquired by EDX. Left to right: sample ablated in air (a), sample ablated in air after 0.5 % KOH treatment (b) and sample ablated in argon ambience (c). The bars in a),b) - 50 μm, c) - 20 μm [P3].

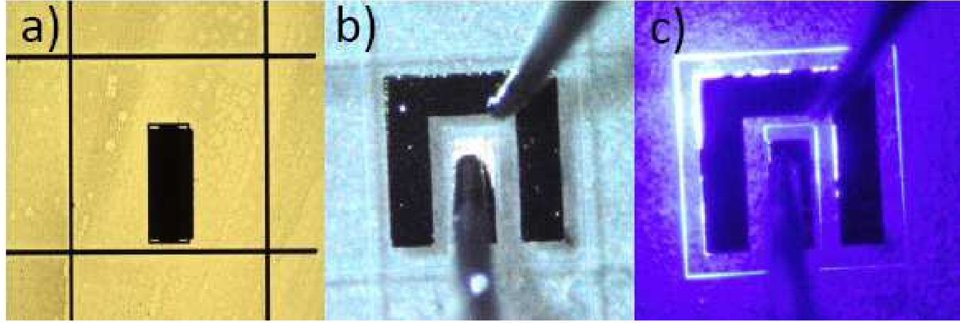

Figure 3.7 Pictures of laser processed LED chip before (a) and after contacts' deposition (b). The LED's electroluminescence is visible on (c). Die feature size is 1x1 mm^2 [P3].

in fully functional LED samples (see Fig. 3.7).

Both LED samples (fabricated by conventional method and our proposed approach) were then electrically and optically characterized. Electrical contacting was realized by probing needles (see Fig. 3.7b,c) onto the p- and n-type contacts, which was when connected to power source (Keithley 2000 Digital Multimeter) for $I-V$ measurements. Light from the LED was collected using focusing lens and optical fiber, which was connected to a CCD spectrometer (OCEAN OPTICS QE65 PRO) for $L-I$ measurements. After the initial $I-V$ and $L-I$ curves have been measured, both samples were then simultaneously annealed using a rapid thermal processing oven (UNITEMP RTP1200-100) in nitrogen ambience at 550°C for 300 seconds. Samples were anneled in order to remove hydrogen atoms from p-type GaN layer, that otherwise makes neutral acceptor-hydrogen complexes [82], that lowers the layer conductivity. After annealing process I-V measurements were repeated for both samples.

3.3 Experimental results

Figure 3.8 shows the current-voltage characteristics in a semi-logarithmic plot for a square device 0.1 cm x 0.1 cm in dimensions with a horseshoe shaped p-contact area approximately $4 \cdot 10^{-3}$ cm^2. The reverse current at -5 V is a useful figure of merit of sample's quality. It is seen from the figure 3.8 that the laser processed device exhibits a leakage current of $2.87 \cdot 10^{-5}$ A before the thermal process. After structure is being annealed the value was $1.58 \cdot 10^{-3}$ A. The leakage currents, in the case of reference sample, were

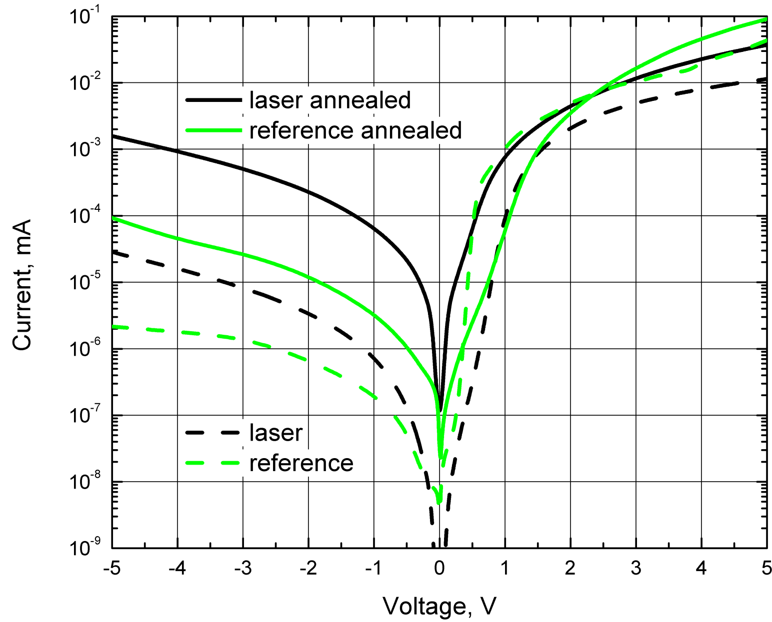

Figure 3.8 Current-voltage characteristics of the LED with mesa-trenches fabricated via fs laser ablation (black) and dry etching (green), as-fabricated (dashed) and after annealing (solid), respectively [P3].

$2.15 \cdot 10^{-6}$ A before and $93 \cdot 10^{-6}$ A after the annealing procedure. Another common figure of merit in the case of LEDs is the forward voltage measured at 20 mA current. A substantial improvement over the whole driving current range for the laser processed LED was observed then structure was annealed, as the voltage dropped to 3.75 V after the thermal acceptor activation, and before that, voltage was above 5 V value and could not been measured. In the case of the reference structure, annealing wasn't influencing results so much, the voltage dropped from 4 V to 3.15 V for as-processed and annealed reference LED samples, respectively. Figure 3.9 shows the corresponding optical output power-current characteristic for the reference sample. Each driving current is represented by a corresponding emission spectra with a peak wavelength around 460 nm. For the highest current of 45 mA a slight redshift is observed.

When comparing the above results of the $I-V$ (see fig. 3.8) characteristics of the reference and the fs laser LED processed from the same epitaxial structure, it is noticeable that parasitic serial resistance of laser machined

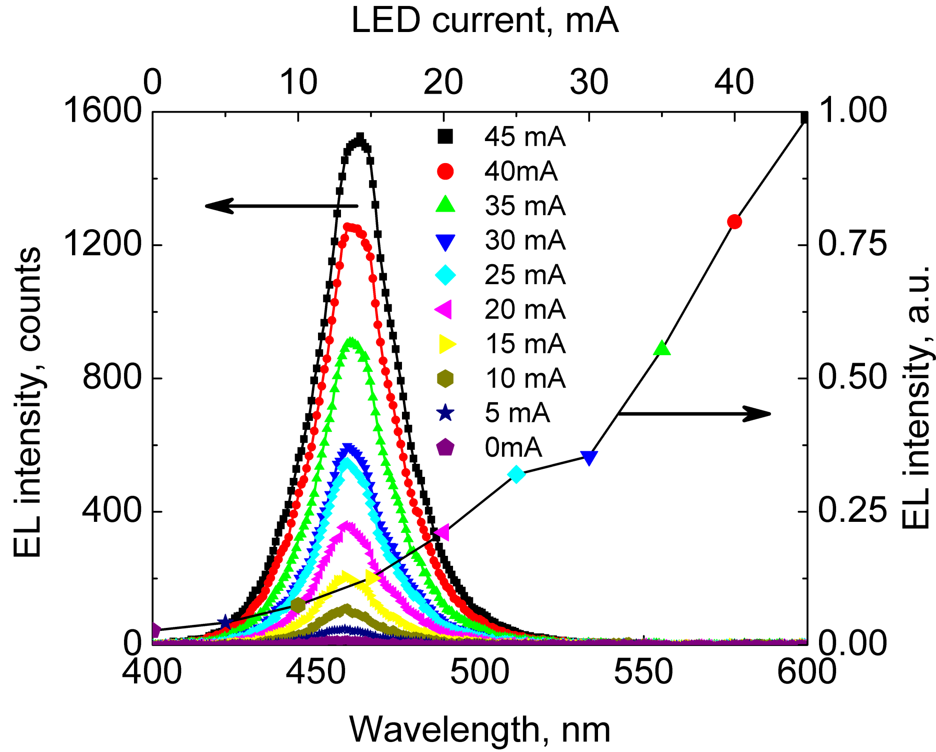

Figure 3.9 LED output spectrum and spectrally integrated output power vs. forward current for the LED with mesa-trenches fabricated by photolithography [P3].

LED was reduced significantly after the annealing and becomes similar in value to a parasitic serial resistance of reference LED before the annealing. Nevertheless, parasitic parallel resistance of laser LED lowers as well, also to a value similar to the conventional devices parallel resistance before the thermal process. For both samples, reverse current has increased after the annealing. This might be explained by a partial degradation of the p-n junction due to the excessive heat. Diminishment of the laser processed sample's parallel parasitic resistance (as well as higher increment of the reverse current) can be explained by GaO or Ga residues redistribution on the inclined side wall of the sample, during the annealing process. This suggests that removal of GaO layer, before contact evaporation, must be done with extra care, however, laser processed devices have been shown to be functional, thus demonstrating the possibility to use such a technological approach for the of devices prototyping. The conventional processing involves two etching processes (chip separation and p-mesa formation), each taking approximately 1 hour (including sample preparation, resist exposure,

etching, resist removal, etc.). The proposed laser processing technique allows performing these two tasks in a single inclined laser ablation process, taking 15-30 min. Therefore this shortens the overall LED processing time by a 30-50 %.

3.4 Conclusions

The use of ultrashort laser pulse ablation enables reducing the number of fundamental processes, critical alignment steps and fabrication time in LED prototyping. *n*-type contacts openings can be fabricated by direct fs laser-processing in an inclined and a self-limiting ablation regime. The forward voltage and the leakage current of such a device have been shown to be comparable to the reference LED sample before the annealing procedure, fabricated using the conventional processing approach. Significantly increased reverse current of the laser machined LED indicates that GaO residues from the ablation process might be limiting the device performance. Molybdenum foil shadow masks obtained by a fs laser ablation, are suitable for contact metal evaporation onto opto-electronic devices.

4. InGaN quantum well LED's ABC recombination coefficients revealed by the small signal frequency domain lifetime measurements

4.1 Introduction

LED internal quantum efficiency is given by an interplay of radiative and non-radiative recombination processes. Most frequently these recombination rates are revealed via TRPL measurements (measuring an emission intensity decay produced by the carrier recombination) [18, 36, 83, 84]. A noticable disadvantage of the method is the variation of non-equilibrium carrier concentration during the measurement, so that it is hard to attribute the measured lifetime to a specific carrier concentration. In addition, the PL intensity decay cannot be considered to be mono-exponential at high pumping levels because of nonlinear dependence of the radiative and Auger recombination rates on the carrier concentration [36, 84]. This complicates the treatment of the measurement data substantially, requiring an accurate physics-based interpretation. This also implies for the research carried out in Lithuania. There are a lot of scientists working on GaN characterization as it was stated in chapter 2, giving their contribution to the world wide debates on GaN research [46, 85, 86]. However most of the published papers are facing a difficulty to evaluate an actual optically pumped non-equilibrium carrier densities within the structure investigated.

For understanding of recombination mechanisms and identifying the main channels of the carrier losses in nitride LEDs, the DLT and its dependence on the LED operating current is much more informative. First, the dependence of DLT on current provides direct information about competition of various recombination channels [87]. Second, in combination with the

current-dependent LED efficiency, DLT enables evaluation of the recombination coefficients related to nonradiative Shockley-Read-Hall (A), bimolecular radiative (B), and Auger (C) recombination channels [88, 89, 90] (not to mixed up with pre-exponential factors used in Eq. (2.1)). The analysis of temperature and emission wavelength dependence of the recombination coefficients enables one to judge on the nature of the dominant microscopic recombination processes in the LED active region [90, 91, 92]. In addition, experimental evaluation of the recombination coefficients allows to estimate the recombination-mediated LED efficiency droop, i.e. non-thermal decline of the LED efficiency at high operating currents. The nature of the droop has been intensively debated for a long time just in terms of the recombination coefficients [93]. In particular, some authors assume the B-coefficient to be independent of the carrier concentration [88, 94, 95, 96] whereas others refer to the band filing with non-equilibrium carriers resulting in the concentration-dependent recombination coefficient [84, 87, 89, 97, 98]. A particular value of the C -coefficient is frequently served as a decisive argument for attributing the LED efficiency droop to the crucial impact of Auger recombination or discarding this recombination channel [93]. Most researchers assume the C-coefficient to be constant, some others regard it as depending on the carrier concentration N [89, 97].

In general, DLT measurements require application of small-signal techniques that combine a certain direct drive current with a time-dependent electrical or optical excitation slightly perturbing the non-equilibrium carrier concentration in the LED active region. Initial attempts to measure DLT involved driving the LED with a DC, which was modulated by a small harmonically AC or pulsed component. The phase difference between the light output and the AC input is then analysed by using the small signal rate equation model to obtain the recombination lifetimes of the carriers [87, 89, 90, 97]. Alternatively, differential carrier lifetime was also measured with purely electrical measurements [88, 99, 100]. By measuring the impedance of the LED with a range of frequencies, an equivalent circuit can be used to obtain the differential resistance and capacitance of the LED. Carrier lifetime was then obtained from the capacitance and differential resistance. However, simulations of the capacitances of typical LED structures have shown that the capacitance originating from the space-charge regions dominates at low currents and becomes comparable with that of the LED

active region at high currents [94]. Therefore, the use of such techniques for the DLT evaluation in III-nitride LEDs may introduce considerable inaccuracies [94, 100]. This was confirmed experimentally while extracting and comparing the carrier lifetime *versus* current density dependence from both methods [100]. Alternatively, deliberately made structures, such as LDs have been investigated in order to extract DLTs in the material, by turn-on delay [95], rate equation analysis [101] or combined approach [96], even measuring the micro-die LEDs bandwidth [98]. Such methods are expensive and difficult to adopt as specific structures must be fabricated.

In order to determine accurately the recombination coefficients, measurements of DLT as a function of forward current are necessary in the widest range possible. For this purpose, the small-signal TRPL (SSTRPL) technique has been proposed, which is based on resonant picosecond optical excitation of the LED active region and monitoring of the optical response decay [94]. An alternative method for the DLT evaluation, which enables expanding the allowable range of the forward currents, could be the FDLM. In this case a harmonic excitation is used and the resulting phase response is measured as a function of modulation frequency [P2]. Both TRPL and FDLM approaches are related via Fourier transform [14], thus provide identical information about the sample. Compared to SSTRPL, the FDLM method does not require a ps laser with a rather small beam size, time-consuming and expensive data acquisition system. An additional advantage of FDLM is an opportunity to analyse the non-linear optical response on the doubled and tripled modulation frequency, relevant to kinetics of radiative and Auger recombination, respectively.

4.1.1 Theoretical background

The interpretation of the DLT data considered here is largely based on the ABC-model frequently used to analyse the recombination mechanisms and, in particular, to explain the droop phenomenon [93, 102]. Assuming the absence of the carrier leakage from the active region, the EQE and current density (J) can be expressed through the non-equilibrium carrier concentration N in the active regions as follows:

$$EQE = \eta_{ext} \frac{BN}{A + BN + CN^2}, \tag{4.1}$$

or

$$J = \mathrm{q}d(AN + BN^2 + CN^3), \tag{4.2}$$

Here η_{ext} is the light extraction efficiency independent of N carrier concentration, d is active region thickness, q is the elementary charge, while A, B, and C correspond to the SRH, radiative and Auger recombination coefficients, respectively. Equations (4.1 and 4.2) determine the EQE dependence on the carrier density parametrically. The number of parameters in the equations, however, is too large to provide reliable and unambiguous fitting of the EQE dependence on the current density. The number of parameters can be significantly reduced if Eq. (4.1) is being rewritten in terms of normalized optical power P (which is LED output power P_{out} normalized to the power P_{max} corresponding to the optical power where EQE gains its maximum value (EQE_{max})) and the dimensionless quality factor $Q = B/(AC)^{1/2}$. In order to evaluate Q (which also enables to evaluate the peak IQE value $IQE_{max} = Q/(Q{+}2)$) there is no need to perform measurements in absolute units. It has been shown [92] that Eq. 4.1 can be rewritten in to:

$$\frac{EQE_{max}}{EQE} = \frac{Q + P^{1/2} + P^{-1/2}}{Q+2}, \tag{4.3}$$

this enables finding the Q-factor directly from the EL measurements. When Q-factor is known, one can describe DLT as:

$$\tau = \frac{1}{A + 2BN + 3CN^2} \text{ [90, 98]} \quad \text{or} \quad \tau = \frac{A^{-1}}{1 + 2QP^{1/2} + 3P} \text{ [94]}. \tag{4.4}$$

allowing to find the SRH coefficient A from the DLT measurements without knowing the actual carrier density function over the driving current $N(I)$. Moreover, when Q and A are known, an evaluation of radiative and Auger coefficients becomes possible as well. Sheet coefficients should be used in the case of QWs, otherwise active region thickness d must be known, which in case of MQW LED is a matter of controversy [94]. The sheet recombination coefficients can be expressed via the evaluated A-coefficient as:

$$B_{2D} = B/d = A^2 Q(2+Q)(\mathrm{q}S/I_{max}) \tag{4.5}$$

and

$$C_{2D} = C/d^2 = A^3(2+Q)^2(\mathrm{q}S/I_{max})^2. \tag{4.6}$$

Here, S is LED active region area and I_{max} the LED operating current corresponding to maximum EQE_{max} value, which is known from the EL data, measured in arbitrary units.

4.2 Experimental setup

4.2.1 Electroluminescence measurements

In order to evaluate the Q-factor, the sample was mounted into a cryostat (CRYO INDUSTRIES 1644-GGS) and preheated to avoid additional internal LED heating, while maintaining forward currents up to 700 mA. The LED was electrically driven by a DC source (KEITHLEY 2000 DIGITAL MULTIMETER) in a wide range of injection currents, ranging from 1 mA to 0.7 A. EL was registrated using a 30 cm focal length monochromator (PRINCETON INSTRUMENTS SPECTRAPRO) and a CCD camera (PIXIS256). The spectrally integrated EL signal was used to calculate EQE in arbitrary units, enabling to find the Q value and calculate the normalized optical output power P.

4.2.2 Small-Signal Differential Carrier Lifetime measurements

For the frequency resolved measurements, experimental setup described in section 2.2 was slightly adapted. The LED sample was mounted and preheated in a cryostat and then was additionally electrically driven by a DC using a current source (KEITHLEY 2000 DIGITAL MULTIMETER), while some carriers have been injected optically directly into QW region using harmonically modulated 405 nm LD as described in section 2.2(see Fig. 4.1). The lifetime measurement range of the setup was from 160 ms to 1.6 ns as described previously. The combined PL and EL signals were dispersed by grating monochromator (JOBIN YVON H10 VIS), ensuring that LD excitation light would not be registered using a PMT. The phase shift between LD modulation and PMT signals was measured as a function of LD modulation frequency. Single frequency sweep time, enabling to measure lifetimes at a single LED driving current, took approximately 10 minutes. As lock-in amplifiers are made to take a small signal from a

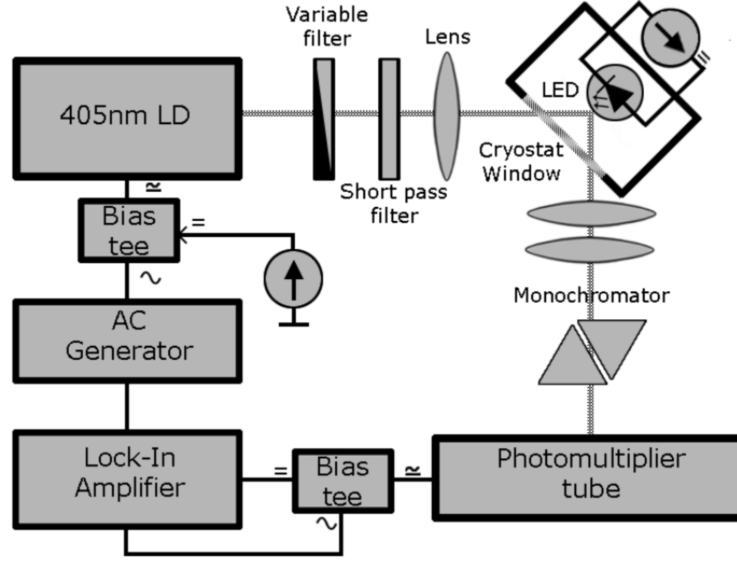

Figure 4.1 Experimental setup used for the small-signal frequency-resolved photoluminescence measurements [P4].

noisy background, long data collection duration was not necessary. The registered signal followed a single exponential decay law confirming that DLT measurement regime was fullfilled. Some in-phase background was also present as in the case of measurements described in chapter 2, so DLTs were extracted by least square-fitting of measured phase shift using equation [35]:

$$\tan\Phi(\omega) = \frac{\frac{S_{gnl}(\omega)}{B_{grnd}(\omega)}\omega\tau_{DLT}}{\frac{S_{gnl}(\omega)}{B_{grnd}(\omega)} + 1 + \omega^2\tau_{DLT}^2}, \tag{4.7}$$

where $\Phi(\omega)$ is detected phase shift, τ_{DLT} is differential carrier lifetime, $S_{gnl}(\omega)$ is time-integrated luminescence intensity, $B_{grnd}(\omega)$ is time-integrated intensity of in-phase background. This equation allows extracting mono-exponential decay in cases when in-phase background cannot be fully avoided (due to LD's parasitic signal in blue spectral region).

Finally, SSTRPL measurement was carried out on the same sample by colleagues from Institut für Festkörperphysik, Technische Universität Berlin and results between these two thechniques were compared. Measurement

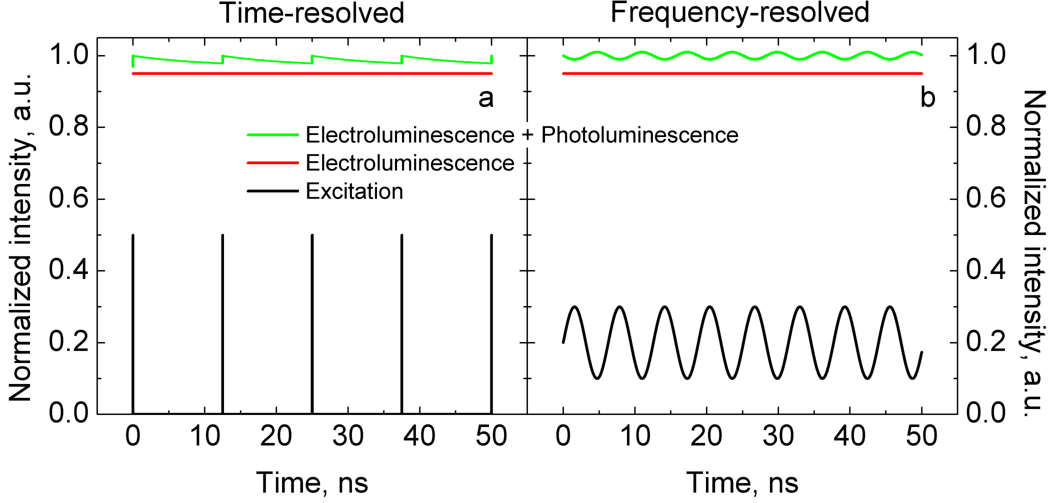

Figure 4.2 Visualisation of SSTRPL (a) and SSFDLM (b) measurements. Excitation intensity (black solid line) is not to scale. [P4]

procedure is described in detail in ref. [94]. Differences between two methods used is best seen when pulsed (SSTRPL) and/or modulated (SSFDLM) photoexcitation is plotted together with electro-luminescence and photoluminescence signals versus time (see Fig. 4.2 a, b).

4.3 Experimental results

From the EL measurements it was confirmed that there was no additional heating of the sample, while going towards higher currents, as experimental results (see Fig. 4.3) could be treated according to the ABC-model (Eq. (4.3)) with a Q value equal to 7.0±0.1 while measuring at 330 K or Q = 7.1±0.1 if measurements are carried out at 315 K. It legitimated the DLT results as any deviation from Eq. (4.4) could not be the artefacts due to the heating of an active area.

Some DLT measurement results with the best fits are shown in figure 4.4 for SSTRPL (a) and three different currents for SSFDLM (b). While DLTs measured as function of the LED normalized optical power P is presented in the figure 4.6. Lifetimes obtained by SSFDLM and SSTRPL techniques match close to ideal, slight mismatch observed might be a result of different probing beam diameter. Indeed, a serious issue for SSTRPL is the signal-to-noise ratio leading to the necessity to use rather narrow laser beams. The beam size of the order of hundred of micrometers can make the

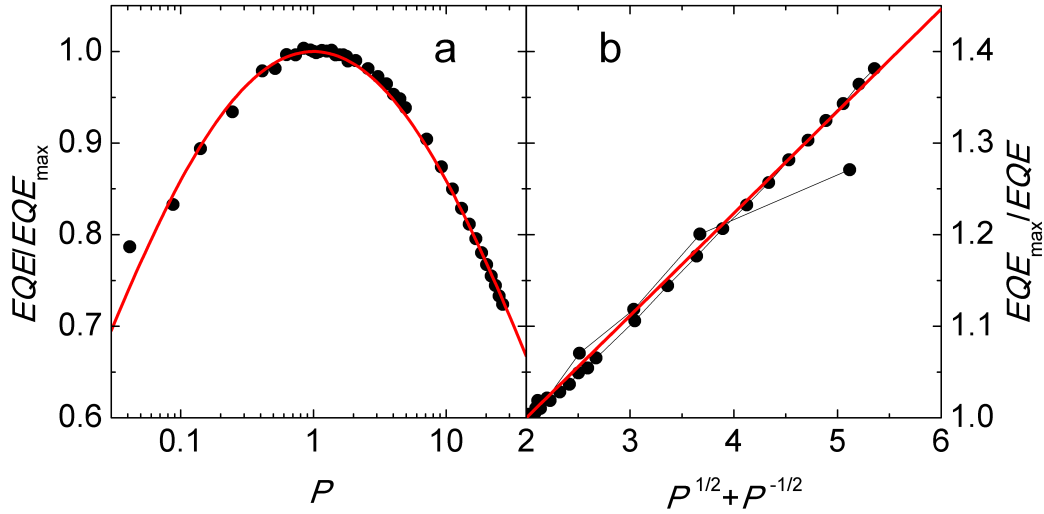

Figure 4.3 EQE/EQE_{max} ratio as function of normalized optical power P (a) and EQE_{max}/EQE ratio as a function of $P^{0.5} + P^{-0.5}$ (b) for the LED sample, measured at 330 K. Dots are experimental points while red solid line is modelling using Eq. (4.3) and $Q = 7.0 \pm 0.1$, which corresponds to a peak IQE value of 77.8 % at a current of 19 mA. Thin black line in (b) is guide for eye. [P4]

DLT measurements position-sensitive because of non-uniform current density distribution in the active region produced by current crowding around the columns of *n*-electrodes (see Fig. 4.5). The use of *quasi*-CW excitation in SSFDLM allows to reduce the demand of peak power density needed to perform the DLT measurements and enabled to cover nearly whole surface of the LED die with the probing LD beam. Consequently the LD excitation peak optical power is much weaker than of the laser used for SSTRPL and the measured DLT is attributed to the mean carrier concentration in the active region rather than to a local one. Indeed, reduced probing position sensitivity while integrating the signal over larger area speaks for the SSFDLM.

Figure 4.6 compares further the DLTs measured by SSTRPL and SSFDLM methods as a function of normalized optical power P. One can see that both methods provide very similar DLT evolution with P. At $P < 4$, the SSFDLM reveal systematic deviation of the DLT behavior from that predicted by the ABC-model: DLT saturates near its value of ∼50 ns at low P. It is important that the SSTRPL data confirm the existence of such deviation (see the point at P ∼0.1 in Fig. 4.6). There may be a number of reasons for

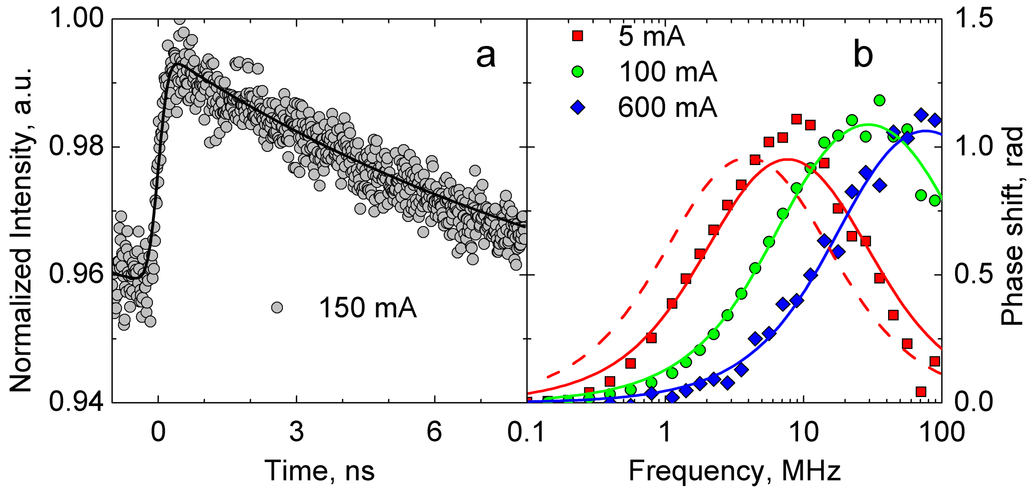

Figure 4.4 Example of acquired experimental results for the LED sample, using SSTRPL @315 K (a) and SSFDLM @330 K (b). In (a) the black solid line represents the best fit using a DLT value of $\tau = (11.1 \pm 0.8)$ ns. In (b) three different drive currents are plotted for comparison: 5 mA (squares), 100 mA (dots) and 600 mA (diamonds), corresponding to normalized optical output power P values of 0.26 ($\tau_{■} = 54.7 \pm 2.7$ ns), 5.2 ($\tau_{●} = 21.5 \pm 0.9$ ns) and 24.8 ($\tau_{◆} = 8.0 \pm 0.6$ ns). Solid lines represents best fits using Eq. (4.7), while dashed line represents modeling using $\tau = 124$ ns (corresponds to open diamond in fig. 4.6). The PL signal in (a) and (b) is bellow 5 % of the total signal. [P4]

Table 4.1 Comparison of recombination coefficients extracted from SSFDLM and SSTRPL measurements [P4]. There was made an assumption that only one quantum well ($d = 3$ nm) is involved in the interaction, then volumetric coefficients were calculated.

Coefficient	SSFDLM	SSTRPL
A, 10^6 s^{-1}	0.91±0.02	1.16±0.03
B_{2D}, 10^{-6} cm^{2}s^{-1}	4.4±0.3	7.3±0.6
B, 10^{-12} cm^{3}s^{-1}	1.3±0.1	2.2±0.2
C_{2D}, 10^{-19} cm^{4}s^{-1}	4.3±0.5	9.2±0.8
C, 10^{-32} cm^{6}s^{-1}	3.9±0.5	8.3±0.7

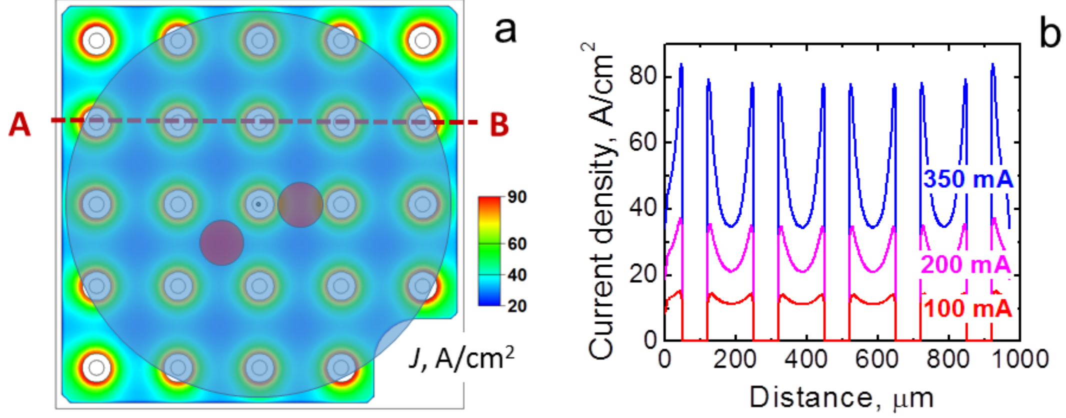

Figure 4.5 Current crowding pattern (top view) of LED die (a). Blue shaded circle indicates beam spot size comparable to one used in SSFDLM measurements, while two red shaded circles indicate beam spot size comparable to one used in SSTRPL measurements in two different possible measurement positions. The cross section A - B view is shown in (b). [P4]

this deviation. First, the ABC-model may no longer fit well the carrier recombination dynamics in the LED active region. In this case, however, it is unclear why the deviation is observed only in the DLT data, whereas the ***EQE*** evolution at such ***P*** still remains well fitted by the model (see Fig. 4.3). One of few possible explanations is that small-signal conditions are not actually met at low ***P*** (current densities). Indeed, it has been shown that TRPL may provide incorrect lifetimes at low currents because of delayed carrier transport to the quantum wells (QW) where they recombine in [99] or the photo-current based control of the small-signal conditions may fail at low currents because of a reduction in the photo-carrier generation efficiency. Another possibility is that the generated carriers leak out of the active region and flow through the LED structure by passing the recombination processes in the active region. So, the DLT saturation lifetime of ~50 ns seen in Fig. 4.6 can be associated in this case with the time specific for the carrier escape from the active region.

Using the measured DLTs, the recombination coefficients A, B and C have been estimated. The A-coefficient was found from fitting the experimental DLT data (Fig. 4.6) by Eq. (4.4); while B_{2D} and C_{2D} coefficients were calculated, using Eqs. (4.5) and (4.6). The results for SSTRPL and SSFDLM are summarized in a Table 4.1. One can see from the table that slight mismatch between the DLT values obtained by both techniques produces

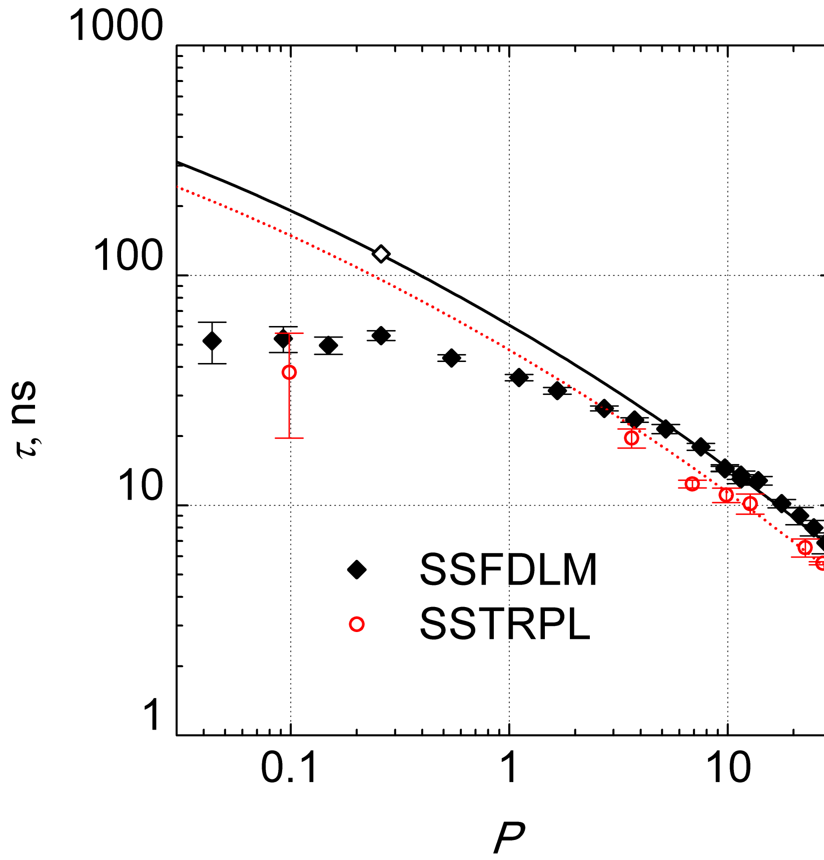

Figure 4.6 SSFDLM (black filled diamonds) and SSTRPL (red open dots) DLT measurement results as a function of normalized LED's optical output power P. Lines represents best fits of the experimental results Eq. (4.4) (black solid line - Q = 7.0, A = (0.91 ± 0.02)·10^6 s^{-1}, red dot line - Q = 7.1, A = (1.16 ± 0.03)·10^6 s^{-1}). Error bars are obtained from least square analysis, results deviation from model are seen in figure 4.4. Open black diamond represent hypothetical fit of the experimental results shown by a dashed line in figure 4.4 b. [P4]

different values of the recombination coefficients. At that, sensitivity of the B_{2D}- and C_{2D}-coefficients to the measured DTLs is higher than it is observed for the A-coefficient, due to their square and cubic dependency on A as seen from Eqs. (4.5) and (4.6).

It is important to notice that the use of SSFDLM enables to reduce the DLT measurement duration at least ten fold in comparison to SSTRPL and to measure the lifetimes in a wider driving current range, due to lock-in amplifier's ability to extract small signal from the noisy backgrounds.

4.4 Conclusions

The small signal frequency domain lifetime measurement technique confirmed its capability of extracting recombination coefficients corresponding to the Shockley-Read-Hall, radiative and Auger recombination channels, while experimental setup being cheaper and more simple to operate in comparison to the commonly used SSTRPL technique. The SSFDLM enables to associate the measured lifetimes with the carrier concentration averaged over the LED active region, which otherwise must be taken into account due to the pronounced current crowding in the LED die. The measurements carried out in a wide range of the normalized optical power P (LED operating current) have revealed a discrepancy between the DLT measured at $P < 4$ and that predicted by the ABC-model underlying the procedure of the recombination coefficient evaluation, thus, measurements should be performed at $P > 4$ in order to extract the ABC-coefficients reliably.

5. Concluding summary

This dissertation is devoted for characterization of GaN epilayers and working LEDs as well as for the fabrication of GaN based LED devices.

The frequency domain lifetime measurement setup provided with a violet laser diode have been proven to be competitive tool for both, GaN LED epi-structures and working devices characterization.

Moreover it was demonstrated that the fs pulse laser ablation in an inclined geometry enables to prototype the GaN LEDs, both cheaper and faster, by diminishing the necessity to make one of fundamental LED processing steps - to etch a chip separation trench.

Bibliography

[1] *http://www.nobelprize.org/nobel_prizes/physics/laureates/*2014/

[2] H.J. Round, A Note on Carborundum, Electr. World. **49**, 309 (1907).

[3] O.V. Losev, Luminous carborundum detector and detection effect and oscillations with crystals, Phil. Mag. **7**(5), 1024 (1928).

[4] Z. Gaviola, Ein Fluorometer. Apparat zur Messung von Fluoreszenzabklingungszeiten, Z. Phys. **42**, 853 (1926).

[5] N. Boens, W. Qin, N. Basaric, J. Hofkens, M. Ameloot, J. Pouget, J.P. Lefevre, B. Valeur, E. Gratton, M. vandeVen, N.D. Silva Jr., Y. Engelborghs, K. Willaert, A. Sillen, G. Rumbles, D. Phillips, A.J.W.G. Visser, A. van Hoek, J.R. Lakowicz, H. Malak, I. Gryczynski, A.G. Szabo, D.T. Krajcarski, N. Tamai, A. Miura, Fluorescence lifetime standards for time and frequency domain fluorescence spectroscopy, Anal. Chem. **79** (5), 2137 (2007).

[6] A.D. Elder, C.F. Kaminski, J.H. Frank, $\varphi 2$ FLIM: a technique for alias-free frequency domain fluorescence lifetime imaging, Opt. Express **17**(25), 23181 (2009).

[7] K.C. Schuermann, H.E. Grecco, flat FLIM: enhancing the dynamic range of frequency domain FLIM, Opt. Express **20**(18), 249 (2012).

[8] H. Chen, E. Gratton, A practical implementation of multifrequency widefield frequency-domain fluorescence lifetime imaging microscopy, Microsc. Res. Techniq. **76**(3), 282 (2013).

[9] J. Sipior, G.M. Carter, J.R. Lakowicz, G. Rao, Blue light-emitting diode demonstrated as an ultraviolet excitation source for nanosecond phase-modulation fluorescence lifetime measurements, Rev. Sci. Instrum. **68**(7), 2666 (1997).

[10] V. Shia, D. Watt, G.W. Faris, High-speed camera with real time processing for frequency domain imaging, Biomed. Opt. Expr. **2**(7), 1931 (2011).

[11] K.H. Shim, B.G. Kim. Simple frequency-domain fluorescence-lifetime measurement system using violet laser diode, J. Korean Phys. Soc. **49**, 647–651 (2006).

[12] A.D. Elder, J.H. Frank, J. Swartling, X. Dai, C.F. Kaminski, Calibration of a wide-field frequency-domain fluorescence lifetime microscopy system using light emitting diodes as light sources, J. Microsc.-Oxford **224**(2), 166 (2006).

[13] T. Mizuno, Y. Mizutani, T. Iwata, Phase-modulation fluorometer using a phase-modulated excitation light source, Opt. Rev. **19**(4), 222 (2012).

[14] W. Becker, *Advanced Time-Correlated Single Photon Counting Techniques* (Springer, Berlin, 2005), pp 20-43.

[15] A.R. Albrecht, R.B. Laghumavarapu, B. Imangholi, M. Sheik-Bahae, K.J. Malloy, Phase fluorometry for semiconductor lifetime measurement, SPIE Proc. **6461**(505), 646108 (2007).

[16] J. Mickevicius, G. Tamulaitis, P. Vitta, A. Zukauskas, M.S. Shur, J. Zhang, J. Yang, R. Gaska, Carrier dynamics in GaN at extremely low excited carrier densities. Solid State Commun., **145**(5–6), 312 (2008).

[17] S.C. Jain, M. Willander, J. Narayan, R. Van Overstraeten, III-nitrides: Growth, characterization, and properties, J. Appl. Phys. **87**(3) 965 (2000).

S.C. Jain, M. Willander, J. Narayan, R. Van Overstraeten, III–nitrides: Growth, characterization, and properties, J. Appl. Phys. **87**, 965 (2000).

[18] M.A. Reshchikov, H. Morkoç, Luminescence properties of defects in GaN, J. Appl. Phys. **97**, 061301 (2005).

[19] J. Mickevičius, J. Jurkevičius, M.S. Shur, J. Yang, R. Gaska, G. Tamulaitis, Photoluminescence efficiency droop and stimulated recombination in GaN epilayers, Opt. Express **20**, 25195 (2012).

[20] A. Vaitkevičius, J. Mickevičius, D. Dobrovolskas, Ö. Tuna, C. Giesen, M. Heuken, G. Tamulaitis, Influence of quantum-confined Stark effect on optical properties within trench defects in InGaN quantum wells with different indium content, J. Appl. Phys. **115**(21), 213512 (2014).

[21] G. Tamulaitis, J. Mickevicius, K. Kazlauskas, A. Zukauskas, M.S. Shur, J. Yang, R. Gaska, Efficiency droop in high-Al-content AlGaN/AlGaN quantum wells, Phys. Status Solidi C **8**, 2130 (2011).

[22] A. Kadys, J. Mickevičius, T. Malinauskas, J. Jurkevičius, M. Kolenda, S. Stanionytė, D. Dobrovolskas, G. Tamulaitis, Optical and structural properties of BGaN layers grown on different substrates, J. Phys. D: Appl. Phys. **48**(46), 25 (2015).

[23] S. Juršėnas, N. Kurilčik, S. Miasojedovas, G. Kurilčik, A. Žukauskas, T. Suski, P. Perlin, M. Leszczynski, P. Prystawko, I. Grzegory, Optical gain in homoepitaxial GaN, Appl. Phys. Lett. **85**, 952 (2004).

[24] E. Gaubas, S. Juršėnas, S. Miasojedovas, J. Vaitkus, A. Žukauskas, Carrier and defect dynamics in photoexcited semi-insulating epitaxial GaN layers, J. Appl. Phys. **96**, 4326 (2004).

[25] G. Tamulaitis, J. Mickevičius, P. Vitta, A. Žukauskas, M.S. Shur, K. Liu, Q. Fareed, J.P. Zhang, R. Gaska, Carrier lifetimes in GaN revealed by studying photoluminescence decay in time and frequency domains, ECS Trans. **3**, 307 (2006).

[26] G. Tamulaitis, J. Mickevičius, P. Vitta, A. Žukauskas, M.S. Shur, Q. Fareed, R. Gaska, Time- and frequency-domain measurements of carrier lifetimes in GaN epilayers, Superlattice. Microst. **40**, 274 (2006).

[27] K. Jarašiūnas, T. Malinauskas, R. Aleksiejūnas, M. Sūdžius, E. Frayssinet, B. Beaumont, J.P. Faurie, P. Gibart, Characterization of differently grown GaN epilayers by time-resolved four-wave mixing technique, Phys. Status Solidi A **202**(4) 566 (2005).

[28] T. Malinauskas, K. Jarašiūnas, S. Miasojedovas, S. Juršėnas, B. Beaumont, P. Gibart, Optical monitoring of nonequilibrium carrier lifetime in freestanding GaN by time-resolved four-wave mixing and photoluminescence techniques, Appl. Phys. Lett. **88**, 202109 (2006).

[29] E. Gaubas, K. Kazlauskas, R. Tomasiunas, J. Vaitkus, A. Zukauskas, Radiation-defect-dependent photoconductivity transients and photoluminescence in semi-insulating GaN, Appl. Phys. Lett. **84**, 5258 (2004).

[30] E. Gaubas, T. Ceponis, A. Jasiunas, V. Kovalevskij, D. Meskauskaite, J. Pavlov, V. Remeikis, A. Tekorius, J. Vaitkus, Correlative analysis of the in situ changes of carrier decay and proton induced photoluminescence characteristics in chemical vapor deposition grown GaN, Appl. Phys. Lett. **104**, 062104 (2014).

[31] P. Malinovskis, A. Mekys, A. Kadys, T. Malinauskas, T. Grinys, V. Bikbajevas, R. Tomašiūnas, J. Storasta, Peculiarities of galvanomagnetic effects in GaN epilayers and GaN/InGaN quantum wells, Phys. Status Solidi C **9**(3-4), 689 (2012).

[32] J. Mickevičius, P. Vitta, G. Tamulaitis, A. Žukauskas, M.S. Shur, J. Zhang, J. Yang, R. Gaška, Luminescence Decay Kinetics in GaN Studied by Frequency Domain Measurements, Acta Phys. Pol. A **113**, 833 (2008).

[33] J.W. Cooley, J.W. Tukey, An algorithm for the machine calculation of complex Fourier series, Math. Comput. **19**(90), 297 (1965).

[34] J.R. Lakowicz, Principles of Fluorescence Spectroscopy, 3rd edn. (Springer, New York, 2006).

[35] P. Vitta, I. Reklaitis, A. Žukauskas, Frequency-domain fluorometry in the presence of high in-phase background, Meas. Sci. Technol. **23**(3), 035502 (2012).

[36] M. Pophristic, F.H. Longa, C. Tran, I.T. Ferguson, R.F. Karlicek Jr., Time-resolved photoluminescence measurements of InGaN light-emitting diodes, Appl. Phys. Lett. **73**(24), 3550 (1998).

[37] G.E.P. Box, Fitting empirical data, Ann. NY Acad. Sci. **86**, 792 (1960).

[38] C. Li, E.B. Stokes, E. Armour, Optical characterization of carrier localization, carrier transportation and carrier recombination in blue-emitting InGaN/GaN MQWs, ECS J. Solid. State Sci. Technol. **4**(2) R10 (2015).

[39] H. Wang, Z. Ji, S. Qu, G. Wang, Y. Jiang, B. Liu, X. Xu, H. Mino, Influence of excitation power and temperature on photoluminescence in InGaN/GaN multiple quantum wells, Opt. Express **20**(4), 3932 (2012).

[40] D. Monroe, Hopping exponential band tails, Phys. Rev. Lett. **54**(2), 146 (1985).

[41] S.D. Baranovskii, R. Eichmann, P. Thomas, Temperature-dependent exciton luminescence in quantum wells by computer simulation, Phys. Rev. B **58**(19), 13081 (1998).

[42] M. Grünewald, B. Movaghar, B. Pohlmann, D. Würtz, Hopping theory of band-tail relaxation in disordered semiconductors, Phys. Rev. B Condens. Matter. **32**(12), 8191 (1985).

[43] Y.H. Cho, G.H. Gainer, A.J. Fischer, J.J. Song, S. Keller, U.K. Mishra, S.P. DenBaars, "S-shaped" temperature-dependent emission shift and carrier dynamics in InGaN/GaN multiple quantum wells, Appl. Phys. Lett. **73**(10), 1370 (1998).

[44] M.S. Minsky, S. Watanabe, N. Yamada, Radiative and nonradiative lifetimes in GaInN/GaN multiquantum wells, J. Appl. Phys. **91**, 5176 (2002).

[45] B. Monemar, B.E. Sernelius, Defect related issues in the "current roll-off" in InGaN based light emitting diodes, Appl. Phys. Lett. **91**, 181103 (2007).

[46] R. Aleksiejūnas, K. Gelžinytė, S. Nargelas, K. Jarašiūnas, M. Vengris, E.A. Armour, D.P. Byrnes, R.A. Arif, S.M. Lee, G.D. Papasouliotis, Diffusion-driven and excitation-dependent recombination rate in blue InGaN/GaN quantum well structures, Appl. Phys. Lett. **104**, 022114 (2014).

[47] J.I. Pankove, E.A. Miller, J.E. Berkeyheiser, GaN Electroluminescent Diodes, RCA Review **32**, 383 (1971).

[48] H. Amano, M. Kito, K. Hiramatsu, I. Akasaki, P-type conduction in Mg-doped GaN treated with low-energy electron beam irradiation (LEEBI), Jap. J. Appl. Phys. **28**, L2112 (1989).

[49] H. Morkoç, S. Strite, G.B. Gao, M.E. Lin, B. Sverdlov, M. Burns, Large-band-gap SIC, Ill-V nitride, and II-VI ZnSe-based semiconductor device technologies, J. Appl. Phys. **76**(3), 1 (1994).

[50] S. Nakamura, T. Mukai, M. Senoh, High-Power GaN P-N Junction Blue-Light-Emitting Diodes, Jap. J. Appl. Phys. **30**(12A), L1998 (1991).

[51] D. Zhuang, J.H. Edgar, Wet etching of GaN, AlN, and SiC: a review, Mater. Sci. Eng. **48** 1 (2005).

[52] S.J. Wang, K.M. Uang, S.L. Chen, Y.C. Yang, S.C. Chang, T.M. Chen, C.H. Chen, Use of patterned laser liftoff process and electroplating nickel layer for the fabrication of vertical-structured GaN-based light-emitting diodes, Appl. Phys. Lett. **87**, 011111 (2005).

[53] H. Masui, S. Nakamura, S.P. Den Baars, U.K. Mishra, Non-polar and semipolar III-nitridelight-emitting diodes: Achievements and challenges, IEEE Trans. Electron Devices **57**(1), 88 (2010).

[54] S.R. Jeon, M.S. Cho, M.A. Yu, G.M. Yang, GaN-based light-emitting diodes using tunnel junctions, IEEE J. Sel. Top. Quant. **8**(4), 739 (2002).

[55] M. Koike, N. Shibata, H. Kato, Y. Takahashi, Development of high efficiency GaN-based multiquantum-well light-emitting diodes and their applications, IEEE J. Sel. Top. Quant. **8**(2), 271 (2002).

[56] L.W. Ji, Y.K. Su, S.J. Chang, C.S. Chang, L.W. Wu, W.C. Lai, X.L. Du, H. Chen, InGaN/GaN multi-quantum dot light-emitting diodes, J. Cryst. Growth **263**(1–4), 114 (2004).

[57] S. Li, A. Waag, GaN based nanorods for solid state lighting, J. Appl. Phys. **111**, 071101 (2012).

[58] V. Jakštas, I. Kašalynas, I. Šimkienė, V. Strazdienė, P. Prystawko, M. Leszczynski, Schottky diodes and high electron mobility transistors of 2DEG AlGaN/GaN structures on sapphire substrate, Lith. J. Phys. **54**(4), 227 (2014).

[59] B.N. Chichkov, C. Momma, S. Nolte, F. von Alvensleben, A. Tünnermann, Femtosecond, picosecond and nanosecond laser ablation of solids, Appl. Phys. A **63**, 109 (1996).

[60] C. Momma, S. Nolte, B.N. Chichkov, F. von Alvensleben, A. Tünnermann, Precise laser ablation with ultrashort pulses, Appl. Surf. Sci. **15**, 109 (1997).

[61] X. Zhu, A.Y. Naumov, D.M. Villeneuve, P.B. Corkum, Influence of laser parameters and material properties on micro drilling with femtosecond laser pulses, Appl. Phys. A **69**, S367 (1999).

[62] E.G. Gamaly, A.V. Rode, B. Luther-Davies, V.T. Tikhonchuk, Ablation of solids by femtosecond lasers: Ablation mechanism and ablation thresholds for metals and dielectrics, Phys. Plasmas **9**, 949 (2002).

[63] A.Y. Vorobyev, C. Guo, Direct femtosecond laser surface nano-microstructuring and its applications. Laser Photon. Rev. **7**, 385 (2013).

[64] C.K. Sun, Y.L. Huang, S. Keller, U.K. Mishra, S.P. DenBaars, Ultrafast electron dynamics study of GaN, Phys. Rev. B **59**, 13535 (1999).

[65] A.J. Fischer, W. Shan, G.H. Park, J.J. Song, D.S. Kim, D.S. Yee, R. Horning, B. Goldenberg, Femtosecond four-wave-mixing studies of nearly homogeneously broadened excitons in GaN, Phys. Rev. B **56**, 1077 (1997).

[66] C.K. Choi, Y.H. Kwon, J.S. Krasinski, G.H. Park, G. Setlur, J.J. Song, Y.C. Chang, Ultrafast carrier dynamics in a highly excited GaN epilayer, Phys. Rev. B **63**, 115315 (2001).

[67] T. Kim, H.S. Kim, M. Hetterich, D. Jones, J.M. Girkin, E. Bente, M.D. Dawson, Femtosecond laser machining of gallium nitride, Mater. Sci. Engineer. B **82**, 262 (2001).

[68] K. Ozono, M. Obara, A. Usui, H. Sunakawa, High-speed ablation etching of GaN semiconductor using femtosecond laser, Opt. Commun. **189**, 103 (2001).

[69] J.T. Chen, W.C. Lai, Y.C. Chang, J.K. Sheu, W.C. Sen, GaN-based light emitting diodes with micro- and nano-patterned structures by femtosecond laser nonlinear decomposition, Appl. Phys. Lett. **101**, 131103 (2012).

[70] J.H. Lee, N.S. Kim, S.S. Hong, J.H. Lee, Enhanced extraction efficiency of InGaN-based light-emitting diodes using 100-kHz femtosecond-laser-scribing technology, IEEE Electron. Dev. Lett. **31**, 213 (2010).

[71] L. Kuna, A. Haase, C. Sommer, E. Zinterl, J.R. Krenn, F.P. Wenzl, P. Pachler, P. Hartmann, S. Tasch, G. Leising, J. Appl. Phys. **104**, 074507 (2008).

[72] T.L. Chang, Z.C. Chen, Y.C. Lee, Micro/nano structures induced by femtosecond laser to enhance light extraction of GaN-based LEDs, Opt. Express **20**, 15997 (2012).

[73] S. Nakashima, K. Sugioka, T. Ito, H. Takai, K. Midorikawa, Fabrication of high-aspect-ratio nanohole arrays on GaN surface by using wet-chemical-assisted femtosecond laser ablation, J. Laser Micro Nanoengineer. **6** 15 (2011).

[74] T. Kudrius, G. Slekys, S. Juodkazis, Surface-texturing of sapphire by femtosecond laser pulses for photonic applications, J. Phys. D: Appl. Phys. **43**, 145501 (2010).

[75] H.Z. Cao, M.L. Zheng, X.Z. Dong, F. Jin, Z.S. Zhao, X.M. Duan, Two-photon nanolithography of positive photoresist thin film with ultrafast laser direct writing, Appl. Phys. Lett. **102**, 201108 (2013).

[76] S. Nakashima, K. Sugioka, K. Midorikawa, Fabrication of microchannels in single-crystal GaN by wet-chemical-assisted femtosecond-laser ablation, Appl. Surf. Sci. **225**, 9770 (2009).

[77] P. Gečys, G. Račiukaitis, E. Miltenis, A. Braun, S. Ragnow, Scribing of thin-film solar cells with picosecond laser pulses, Phys. Procedia. **12**, 141 (12).

[78] R. Moser, M. Kunzer, C. Gossler, R. Schmidt, K. Köhler, W. Pletschen, U.T. Schwarz, J. Wagner, Laser processing of GaN-based LEDs with ultraviolet picosecond laser pulses. Proc. SPIE **8433**,84330Q (2012).

[79] R. Moser, C. Gossler, M. Kunzer, K. Köhler, W. Pletschen, J. Brunne, U.T. Schwarz, J. Wagner, Laser direct writing of GaN-based light-emitting diodes - The suitable laser source for mesa definition, J. Appl. Phys. **113**, 103107 (2013).

[80] J.F. Shackelford, W. Alexander, J.S. Park, The CRC materials science and engineering handbook, 2nd edn. (CRC Press, Boca Raton, 1994).

[81] S.I. Stepanov, V.I. Nikolaev, V.E. Bougrov and A.E. Romanov, Gallium oxide: Properties and applications - A review, Rev. Adv. Mater. Sci. **44**(1), 63 (2016).

[82] S. Nakamura, N. Iwasa, M. Senoh, T. Mukai, Hole compensation mechanism of p-type GaN films, Jpn. J. Appl. Phys. **31**(5A), 1258 (1992).

[83] H. Kim, D.S. Shin, H.Y. Ryu, J.I. Shim, Analysis of time-resolved photoluminescence of InGaN quantum wells using the carrier rate equation, Jpn. J. App. Phys. **49**, 112402 (2010).

[84] Ž. Podlipskas, R. Aleksiejūnas, A. Kadys, J. Mickevičius, J. Jurkevičius, G. Tamulaitis, M. Shur, M. Shatalov, J. Yang, R. Gaska, Dependence of radiative and nonradiative recombination on carrier density and Al content in thick AlGaN epilayers, J. Phys. D: Appl. Phys. **49**, 145110 (2016).

[85] S. Krotkus, S. Miasojedovas, S. Juršėnas, Threshold of stimulated emission in GaN layers grown by various techniques, Physica B: Condens. Matter. Vol. **450**, 16 (2014).

[86] G. Tamulaitis, J. Mickevičius, K. Kazlauskas, A. Žukauskas, M.S. Shur, J. Yang, R. Gaska, Efficiency droop in high-Al-content AlGaN/AlGaN quantum wells, Phys. Status Solidi C **8**, 2130 (2011).

[87] P.G. Eliseev, M. Osin'ski, H. Li, I.V. Akimova, Recombination balance in green-light-emitting GaN/InGaN/AlGaN quantum wells, Appl. Phys. Lett. **75**, 24 (1999).

[88] M. Meneghini, N. Trivellin, G. Meneghesso, E. Zanoni, U. Zehnder, B. Hahn, A combined electro-optical method for the determination of the recombination parameters in InGaN-based light-emitting diodes, Appl. Phys. Lett. **106**, 114508 (2009).

[89] A. David, M.J. Grundmann, Droop in InGaN light-emitting diodes: A differential carrier lifetime analysis, Appl. Phys. Lett. **96**, 103504 (2010).

[90] B. Galler, P. Drechsel, R. Monnard, P. Rode, P. Stauss, S. Froehlich, W. Bergbauer, M. Binder, M. Sabathil, B. Hahn, J. Wagner, Influence of indium content and temperature on Auger-like recombination in InGaN quantum wells grown on (111) silicon substrates, Appl. Phys. Lett. **101**, 131111 (2012).

[91] D. Schiavon, M. Binder, M. Peter, B. Galler, P. Drechsel, F. Scholz, Wavelength-dependent determination of the recombination rate coefficients in single-quantum-well GaInN/GaN light emitting diodes, Phys. Status Solidi B **250**(2), 283 (2013).

[92] I.E. Titkov, S.Y. Karpov, A. Yadav, V.L. Zerova, M. Zulonas, B. Galler, M. Strassburg, I. Pietzonka, H.J. Lugauer, E.U. Rafailov, Temperature-Dependent Internal Quantum Efficiency of Blue High-Brightness Light-Emitting Diodes, IEEE J. Quant. Electron. **50**, 911 (2014).

[93] J. Piprek, Efficiency droop in nitride-based light-emitting diodes, Phys. Status Solidi A **207**(10), 2217(2010).

[94] F. Nippert, S. Karpov, I. Pietzonka, B. Galler, A. Wilm, T. Kure, C. Nenstiel, G. Callsen, M. Strassburg, H.J. Lugauer, A. Hoffmann, Determination of recombination coefficients in InGaN quantum-well light-emitting diodes by small-signal time-resolved photoluminescence, Jpn. J. Appl. Phys. **55**, 05FJ01 (2016).

[95] M. Zhang, P. Bhattacharya, J. Singh, J. Hinckley, Direct measurement of auger recombination in In0.1Ga0.9N/GaN quantum wells and its impact on the efficiency of In0.1Ga0.9N/GaN multiple quantum well light emitting diodes, Appl. Phys. Lett. **95**, 201108 (2009).

[96] W.G. Scheibenzuber, U.T. Schwarz, L. Sulmoni, J. Dorsaz, J.F. Carlin, N. Grandjean, Recombination coefficients of GaN-based laser diodes, Appl. Phys. Lett. **109**, 093106 (2011).

[97] A. David, M.J. Grundmann, Influence of polarization fields on carrier lifetime and recombination rates in InGaN-based light-emitting diodes, Appl. Phys. Lett. **97**, 033501 (2010).

[98] R.P. Green, J.J.D. McKendry, D. Massoubre, E. Gu, M.D. Dawson, A.E. Kelly, Modulation bandwidth studies of recombination processes in blue and green InGaN quantum well micro-light-emitting diodes, Appl. Phys. Lett. **102**, 091103 (2013).

[99] G.E. Shtengel, D.A. Ackerman, P.A. Morton, True carrier lifetime measurements of semiconductor lasers, Electron. Lett. **31**, 20 (1995).

[100] L. Riuttanen, P. Kivisaari, N.Mäntyoja, J. Oksanen, M. Ali, S. Suihkonen, M. Sopanen, Recombination lifetime in InGaN/GaN based light emitting diodes at low current densities by differential carrier lifetime analysis, Phys. Status Solidi C **10**(3), 327 (2013).

[101] H. Yoshida, M. Kuwabara, Y. Yamashita, K. Uchiyama, H. Kan, Radiative and nonradiative recombination in an ultraviolet GaN/AlGaN multiple-quantum-well laser diode, Appl. Phys. Lett. **96**, 211122 (2010).

[102] Q. Dai, Q. Shan, J. Wang, S. Chhajed, J. Cho, E.F. Schubert, M.H. Crawford, D.D. Koleske, M.H. Kim, Y. Park, Carrier recombination mechanisms and efficiency droop in GaInN/GaN light-emitting diodes, Appl. Phys. Lett. **97**, 133507 (2010).

[103] X. Guo, E.F. Schubert, Current crowding in GaN/InGaN light emitting diodes on insulating substrates, J. Appl. Phys. **90**(8), 4191 (2001).